

Dynamic Spatial Treatment Effects as Continuous Functionals: Theory and Evidence from Healthcare Access

Tatsuru Kikuchi*

*Faculty of Economics, The University of Tokyo,
7-3-1 Hongo, Bunkyo-ku, Tokyo 113-0033 Japan*

(October 20, 2025)

Abstract

I develop a continuous functional framework for spatial treatment effects grounded in Navier-Stokes partial differential equations. Rather than discrete treatment parameters, the framework characterizes treatment intensity as continuous functions $\tau(\mathbf{x}, t)$ over space-time, enabling rigorous analysis of boundary evolution, spatial gradients, and cumulative exposure. Empirical validation using 32,520 U.S. ZIP codes demonstrates exponential spatial decay for healthcare access ($\kappa = 0.002837$ per km, $R^2 = 0.0129$) with detectable boundaries at 37.1 km. The framework successfully diagnoses when scope conditions hold: positive decay parameters validate diffusion assumptions near hospitals, while negative parameters correctly signal urban confounding effects. Heterogeneity analysis reveals $2\text{-}13 \times$ stronger distance effects for elderly populations and substantial education gradients. Model selection strongly favors logarithmic

*e-mail: tatsuru.kikuchi@e.u-tokyo.ac.jp

decay over exponential ($\Delta\text{AIC} > 10,000$), representing a middle ground between exponential and power-law decay. Applications span environmental economics, banking, and healthcare policy. The continuous functional framework provides predictive capability ($d^*(t) = \xi^* \sqrt{t}$), parameter sensitivity ($\partial d^*/\partial \nu$), and diagnostic tests unavailable in traditional difference-in-differences approaches.

Keywords: Spatial treatment effects, continuous functionals, Navier-Stokes equations, healthcare access, spatial boundaries, heterogeneous treatment effects

JEL Classification: C14, C21, C31, I14, R12

Contents

1	Introduction	6
1.1	Motivation and Context	6
1.2	Main Contributions	7
1.3	Roadmap	8
2	Literature Review	9
2.1	Spatial Econometric Methods	9
2.2	Treatment Effect Heterogeneity and Boundaries	10
2.3	Spatial Spillovers and General Equilibrium	11
2.4	My Recent Contributions to Spatial Treatment Effect Boundaries	11
3	Theoretical Framework	12
3.1	Treatment Intensity as Continuous Functional	13
3.2	Derivation of Governing Equation	14
3.2.1	Mass Conservation	14
3.2.2	Constitutive Relations	14
3.2.3	Differential Form	15
3.3	Boundary Conditions and Well-Posedness	15
3.4	Self-Similar Solutions	16
3.5	Steady-State Solutions	17
3.5.1	Pure Diffusion from Point Source	17
3.5.2	Exponential Modification	17
3.6	Spatial Boundary Definition and Properties	18
3.7	Dynamic Boundary Evolution	19

3.8	Cumulative Exposure Functional	20
3.9	Parameter Sensitivity Analysis	21
3.10	Gradient Fields and Intensive Margin	22
3.11	Summary of Theoretical Framework	23
4	Data and Empirical Strategy	23
4.1	Data Sources	23
4.2	Distance Calculation	24
4.3	Empirical Specification	24
4.4	Heterogeneity Analysis	25
5	Main Results	25
5.1	Descriptive Statistics and Spatial Patterns	26
5.2	Baseline Exponential Decay Estimates	28
5.2.1	ZCTA-Level Results (Primary Analysis)	29
5.2.2	County-Level Results (Robustness)	31
5.3	Detailed Analysis: ACCESS2 at ZCTA Level	32
5.4	Model Comparison: Exponential vs Power-Law vs Logarithmic	36
5.5	Diagnostic Capability: When Does the Framework Apply?	40
5.6	Summary of Main Results	42
6	Comparison to Traditional Methods	43
6.1	Conceptual Comparison	43
6.2	Empirical Comparison	45
6.2.1	Traditional DiD Results	47
6.2.2	Navier-Stokes Results (Same Data)	49

6.3	Strengths and Limitations	50
6.3.1	Navier-Stokes Advantages	50
6.3.2	Navier-Stokes Limitations	51
6.3.3	Traditional DiD Advantages	51
6.3.4	Traditional DiD Limitations	52
6.4	When to Use Each Approach	53
6.5	Empirical Recommendation	54
7	Conclusion	54
7.1	Summary of Main Findings	55
7.2	Theoretical Contributions	57
7.3	Methodological Contributions	57
7.4	Comparison to Related Literatures	59
7.5	Policy Implications	60
7.6	Limitations and Future Research	61
7.7	Broader Implications	63
7.8	Final Remarks	64

1 Introduction

Treatment effects in economics are conventionally represented as scalar parameters—average treatment effects (ATE), treatment on the treated (ATT), local average treatment effects (LATE). While appropriate for many settings, these discrete representations obscure the continuous nature of treatment propagation through space and time. When hospitals open, bank branches establish, or infrastructure is built, economic impacts do not manifest as step functions at arbitrary cutoffs. Instead, treatment intensity varies smoothly across geographic space, evolves continuously over time, and exhibits rich mathematical structure arising from underlying diffusion processes.

This paper develops a framework for *dynamic spatial treatment effects as continuous functionals* defined over space-time domains. Rather than estimating point parameters, the framework characterizes treatment intensity as continuous functions $\tau : \mathbb{R}^d \times \mathbb{R}_+ \rightarrow \mathbb{R}$ satisfying partial differential equations (PDEs) that govern propagation dynamics. This functional perspective enables rigorous analysis of objects beyond the reach of discrete estimators: boundary evolution rates, spatial gradients, cumulative exposure integrals, and sensitivity functionals.

1.1 Motivation and Context

The motivation for continuous functional definitions comes from recognizing that treatment propagation follows physical principles. Just as heat diffuses continuously from sources according to the heat equation, economic treatments—healthcare accessibility, bank services, infrastructure benefits—spread through space following diffusion-advection dynamics. The mathematical structure is captured by the Navier-Stokes system:

$$\frac{\partial \tau}{\partial t} + (\mathbf{v} \cdot \nabla) \tau = \nu \nabla^2 \tau + S(\mathbf{x}, t) \quad (1)$$

where $\tau(\mathbf{x}, t)$ represents treatment intensity at location \mathbf{x} and time t , \mathbf{v} is the velocity field, ν is the diffusion coefficient, and $S(\mathbf{x}, t)$ represents source emissions.

To validate this framework, I analyze healthcare access using 32,520 U.S. ZIP codes (ZCTAs). The empirical results strongly support theoretical predictions: healthcare access exhibits exponential spatial decay with decay parameter $\kappa = 0.002837$ per kilometer (SE = 0.000155, $p < 0.001$). The model explains 1.29% of spatial variation, modest but meaningful given the complexity of healthcare access determinants. For the median ZCTA, effects extend to a spatial boundary of 37.1 km (95% CI: [33.2, 41.1] km) at the 10% threshold.

1.2 Main Contributions

This paper makes four main contributions:

First, theoretically, I establish a unified mathematical framework showing how spatial boundaries emerge from Navier-Stokes equations. Building on my prior work (Kikuchi, 2024a,c,f), the framework provides:

- Continuous functional definitions: $\tau(\mathbf{x}, t)$, $d^*(t)$, $v(t) = \partial d^*/\partial t$
- Self-similar solutions: $\tau(r, t) = t^{-\alpha} f(r/t^\beta)$
- Parameter sensitivity: $\partial d^*/\partial \nu$ for policy analysis
- Cumulative exposure: $\Phi(\mathbf{x}) = \int_0^T \tau(\mathbf{x}, t) dt$

Second, methodologically, I develop diagnostic procedures for assessing scope conditions, extending my nonparametric identification work (Kikuchi, 2024d,e):

- Sign reversal test: positive κ validates diffusion, negative signals confounding
- R^2 magnitude: distinguishes dominant versus secondary mechanisms
- Regional heterogeneity: identifies where framework applies versus fails
- Model selection: AIC/BIC for exponential vs power-law vs logarithmic decay

Third, empirically, I demonstrate applicability across healthcare outcomes, complementing my stochastic boundary work (Kikuchi, 2024b):

- ACCESS2: Strong decay ($\kappa = 0.002837$, boundary = 37.1 km)
- OBESITY: Weak decay ($\kappa = 0.000346$, boundary = 304.4 km)
- DIABETES: Negative decay (framework correctly rejects)

Model comparison reveals logarithmic decay outperforms exponential ($\Delta AIC > 10,000$), representing diminishing marginal effects of distance.

Fourth, for policy, heterogeneity analysis reveals substantial variation:

- Age: 2-13x stronger effects for elderly populations
- Education: High education reduces distance sensitivity 5-13x
- Implications: Target elderly + low-education rural populations

1.3 Roadmap

The remainder of the paper proceeds as follows. Section 2 provides a comprehensive literature review situating this work within spatial econometrics, treatment effects, and my recent contributions. Section 3 presents the complete theoretical framework, deriving the governing

PDE from first principles and establishing existence and uniqueness of solutions. Section 4 describes data and empirical strategy. Section 5 presents main results. Section ?? analyzes heterogeneity. Section 6 compares with traditional methods. Section 7 concludes.

2 Literature Review

This paper contributes to several literatures in spatial econometrics, treatment effects, and causal inference with spillovers. I organize the review around four themes: (1) spatial econometric methods, (2) treatment effect heterogeneity and boundaries, (3) spatial spillovers and general equilibrium, and (4) my recent contributions to spatial treatment effect boundaries.

2.1 Spatial Econometric Methods

The foundational work in spatial econometrics is Anselin (1988), who developed methods for estimating spatial lag and spatial error models. Cliff and Ord (1981) provided early treatments of spatial autoregressive processes. More recently, Conley (1999) developed GMM estimators robust to unknown forms of spatial correlation, establishing the standard approach for spatial standard errors used in this paper.

Recent advances focus on inference robust to spatial correlation. Müller and Watson (2022) develop theory for spatial correlation robust inference when the spatial correlation structure is unknown and potentially strong. They show that conventional spatial HAC standard errors can fail when spatial correlation is long-range, and propose alternative inference procedures. Müller and Watson (2024) extend this to spatial unit roots and spurious regression, showing that spatial correlation can induce spurious findings analogous to time series unit roots. My framework complements these by deriving spatial correlation structures

from physical diffusion processes rather than imposing them statistically.

Kelly et al. (2019) study spatial variation in economic outcomes using high-dimensional methods. Delgado and Robinson (2014) develop tests for spatial effects in nonparametric regressions. My approach differs by grounding spatial patterns in PDEs from mathematical physics rather than treating them as nuisance parameters.

2.2 Treatment Effect Heterogeneity and Boundaries

The modern treatment effects literature emphasizes heterogeneity. Imbens and Rubin (2015) provide comprehensive treatment of heterogeneous treatment effects in experimental and quasi-experimental settings. Athey and Imbens (2017) survey machine learning methods for estimating conditional average treatment effects (CATE). Chernozhukov et al. (2018) develop generic machine learning inference for causal effects including heterogeneous effects.

For spatial treatments specifically, Butts and Gardner (2023) formalize spatial spillovers in difference-in-differences, showing how to identify and estimate treatment effects when spillovers are present. Delgado et al. (2021) develop bounds for treatment effects under spatial interference. My framework differs by providing explicit functional forms for spatial decay rather than nonparametric bounds.

In healthcare specifically, Currie and Reagan (2003) document that distance to hospitals affects health outcomes, while Buchmueller et al. (2006) study hospital closures. Currie and Neidell (2005) examine air pollution and health using spatial variation. My contribution is providing rigorous boundary identification grounded in physical diffusion rather than ad hoc distance cutoffs.

2.3 Spatial Spillovers and General Equilibrium

A growing literature studies spatial spillovers in general equilibrium settings. Monte et al. (2018) study commuting and spatial equilibrium. Allen and Arkolakis (2014) develop quantitative spatial models of trade. Redding and Rossi-Hansberg (2017) survey spatial economics with emphasis on trade and agglomeration.

Heblich et al. (2021) study pollution effects using German reunification, documenting spatial spillovers. Hsiang et al. (2019) estimate spatial spillovers in climate impacts. My stochastic boundary framework (Kikuchi, 2024b) extends these by incorporating general equilibrium feedbacks into the boundary identification process.

2.4 My Recent Contributions to Spatial Treatment Effect Boundaries

This paper builds on my recent work developing continuous functional frameworks for spatial treatment effects. I briefly summarize these contributions:

Kikuchi (2024a) establishes the unified theoretical framework for spatial and temporal treatment effect boundaries. That paper proves existence and uniqueness of boundary solutions under general diffusion-advection dynamics, establishes convergence rates for boundary estimators, and provides identification conditions. The current paper applies this theory to healthcare access.

Kikuchi (2024b) develops stochastic boundary methods for spatial general equilibrium with spillovers. When treatment effects feedback into location decisions, boundaries become stochastic rather than deterministic. That paper shows how to estimate boundary distributions using kernel methods and applies the framework to housing markets. The healthcare

application here focuses on partial equilibrium settings where feedback effects are minimal.

Kikuchi (2024c) derives spatial and temporal boundaries from Navier-Stokes equations specifically for difference-in-differences settings. That paper focuses on panel data with time-varying treatments, while this paper emphasizes cross-sectional analysis and model selection.

Kikuchi (2024d) provides nonparametric identification and estimation of spatial boundaries using 42 million pollution observations. That paper develops kernel-based methods that do not assume functional forms for decay. The current paper focuses on parametric exponential/logarithmic models and their relative performance.

Kikuchi (2024e) applies nonparametric boundary identification to bank branch consolidation, finding negative decay parameters that correctly signal urban confounding. This demonstrates the diagnostic capability of the framework—it identifies when diffusion assumptions hold versus when they fail. The healthcare application here similarly shows diagnostic capability.

Kikuchi (2024f) (the current paper) focuses on dynamic boundary evolution with continuous functionals. The emphasis is on healthcare access heterogeneity and model selection between exponential, power-law, and logarithmic decay.

Together, these papers establish continuous functional methods as a comprehensive approach to spatial causal inference, with applications spanning environmental economics, banking, and healthcare.

3 Theoretical Framework

This section presents the complete theoretical framework, deriving the governing PDE from first principles and establishing key mathematical properties. I build on my prior theoretical

work (Kikuchi, 2024a,c) while providing self-contained exposition.

3.1 Treatment Intensity as Continuous Functional

The foundation rests on defining treatment effects as continuous functions over space-time rather than discrete parameters.

Definition 3.1 (Treatment Intensity Functional). *The **treatment intensity field** is a continuous function $\tau : \mathcal{D} \times \mathbb{R}_+ \rightarrow \mathbb{R}$ where $\mathcal{D} \subseteq \mathbb{R}^d$ is the spatial domain and \mathbb{R}_+ is the positive time axis, satisfying:*

$$\tau(\mathbf{x}, t) = \lim_{r \rightarrow 0} \frac{1}{|\mathcal{B}_r(\mathbf{x})|} \int_{\mathcal{B}_r(\mathbf{x})} u(\mathbf{y}, t) d\mathbf{y} \quad (2)$$

where $u(\mathbf{y}, t)$ is microscopic treatment intensity and $\mathcal{B}_r(\mathbf{x})$ is a ball of radius r with volume $|\mathcal{B}_r(\mathbf{x})|$.

Interpretation: The field $\tau(\mathbf{x}, t)$ represents the continuum limit of treatment concentration, analogous to density fields in fluid mechanics. At each location \mathbf{x} and time t , τ measures local treatment exposure intensity. The microscopic-to-macroscopic transition via spatial averaging ensures τ is well-defined and smooth under regularity conditions.

Remark 3.1. Definition 3.1 formalizes the notion that economic treatments propagate as continuous fields rather than discrete jumps. This is natural for:

- Healthcare: Access probability (visits per capita)
- Pollution: Concentration ($\mu\text{g}/\text{m}^3$)
- Banking: Service availability (branches per capita)
- Information: Technology adoption rates

3.2 Derivation of Governing Equation

I derive the governing PDE from mass conservation and constitutive relations.

3.2.1 Mass Conservation

Consider a control volume $\mathcal{V} \subset \mathcal{D}$ with boundary $\partial\mathcal{V}$. The total treatment mass is:

$$M(t) = \int_{\mathcal{V}} \tau(\mathbf{x}, t) d\mathbf{x} \quad (3)$$

Mass balance states:

$$\frac{dM}{dt} = - \int_{\partial\mathcal{V}} \mathbf{J} \cdot \mathbf{n} dA + \int_{\mathcal{V}} S(\mathbf{x}, t) d\mathbf{x} \quad (4)$$

where \mathbf{J} is the flux vector, \mathbf{n} is the outward normal, and S represents sources/sinks.

3.2.2 Constitutive Relations

The flux consists of advective and diffusive components:

$$\mathbf{J} = \mathbf{v}\tau - \nu \nabla \tau \quad (5)$$

where:

- $\mathbf{v}\tau$: Advective flux (bulk motion)
- $-\nu \nabla \tau$: Diffusive flux (Fick's law)
- $\nu > 0$: Diffusion coefficient

3.2.3 Differential Form

Applying the divergence theorem:

$$\int_{\mathcal{V}} \frac{\partial \tau}{\partial t} d\mathbf{x} = - \int_{\mathcal{V}} \nabla \cdot \mathbf{J} d\mathbf{x} + \int_{\mathcal{V}} S d\mathbf{x} \quad (6)$$

Since \mathcal{V} is arbitrary:

$$\frac{\partial \tau}{\partial t} + \nabla \cdot (\mathbf{v} \tau) = \nu \nabla^2 \tau + S(\mathbf{x}, t) \quad (7)$$

For incompressible flow ($\nabla \cdot \mathbf{v} = 0$):

$$\frac{\partial \tau}{\partial t} + (\mathbf{v} \cdot \nabla) \tau = \nu \nabla^2 \tau + S(\mathbf{x}, t) \quad (8)$$

This is the *advection-diffusion equation*, a special case of the Navier-Stokes system for passive scalar transport.

3.3 Boundary Conditions and Well-Posedness

Assumption 3.1 (Boundary Conditions). *The treatment field satisfies:*

1. *Initial condition:* $\tau(\mathbf{x}, 0) = \tau_0(\mathbf{x})$ with $\tau_0 \in L^2(\mathcal{D})$
2. *Far-field decay:* $\lim_{|\mathbf{x}| \rightarrow \infty} \tau(\mathbf{x}, t) = 0$ for all $t > 0$
3. *Source regularity:* $S(\mathbf{x}, t) \in L^2(\mathcal{D} \times [0, T])$ for all finite T

Theorem 3.1 (Existence and Uniqueness). *Under Assumption 3.1, the advection-diffusion equation (8) admits a unique weak solution $\tau \in L^2(0, T; H^1(\mathcal{D}))$ for any finite time horizon $T < \infty$.*

Proof Sketch. Standard energy methods. Multiply (8) by τ and integrate over \mathcal{D} :

$$\frac{1}{2} \frac{d}{dt} \int_{\mathcal{D}} \tau^2 d\mathbf{x} + \nu \int_{\mathcal{D}} |\nabla \tau|^2 d\mathbf{x} = \int_{\mathcal{D}} S \tau d\mathbf{x} \quad (9)$$

The advection term vanishes for incompressible flow. Apply Cauchy-Schwarz and Gronwall's inequality to obtain energy bounds. Uniqueness follows from energy estimates on the difference of two solutions. See Evans (2010) Chapter 7 for complete proof. \square

3.4 Self-Similar Solutions

For diffusion problems without advection ($\mathbf{v} = 0$) and with initial point source, solutions exhibit self-similarity.

Proposition 3.1 (Self-Similar Form). *For point source $S(\mathbf{x}, t) = Q\delta(\mathbf{x})\delta(t)$, the solution to the diffusion equation $\partial\tau/\partial t = \nu\nabla^2\tau$ in \mathbb{R}^d takes the form:*

$$\tau(r, t) = \frac{Q}{(4\pi\nu t)^{d/2}} \exp\left(-\frac{r^2}{4\nu t}\right) \quad (10)$$

where $r = |\mathbf{x}|$.

Proof. The fundamental solution (Green's function) for the heat equation in \mathbb{R}^d is well-known. Dimensional analysis suggests $\tau \sim t^{-d/2} f(r/\sqrt{t})$. Substituting into the PDE yields an ODE for f whose solution is the Gaussian. See Crank (1979) for details. \square

Implication: Solutions spread as $\sim \sqrt{t}$, not linearly. The scaling $d^*(t) \propto \sqrt{t}$ is a fundamental feature of diffusion.

3.5 Steady-State Solutions

For time-independent sources and long times, the system reaches steady state: $\partial\tau/\partial t = 0$.

3.5.1 Pure Diffusion from Point Source

Consider $\nu\nabla^2\tau = -Q\delta(\mathbf{x})$ in \mathbb{R}^3 with $\tau \rightarrow 0$ as $r \rightarrow \infty$. In spherical coordinates:

$$\nu \frac{1}{r^2} \frac{d}{dr} \left(r^2 \frac{d\tau}{dr} \right) = 0 \quad (11)$$

This yields:

$$\tau(r) = \frac{A}{r} + B \quad (12)$$

Applying boundary conditions: $B = 0$ and $A = Q/(4\pi\nu)$, giving:

$$\tau(r) = \frac{Q}{4\pi\nu r} \quad (13)$$

This exhibits $1/r$ power-law decay.

3.5.2 Exponential Modification

In practice, exponential decay emerges from:

1. Finite source extent (not true point source)
2. Decay/absorption: $\nu\nabla^2\tau - \lambda\tau = -S(\mathbf{x})$
3. Bounded domains with absorbing boundaries

For the modified equation $\nu\nabla^2\tau - \lambda\tau = -Q\delta(\mathbf{x})$, the solution is:

$$\tau(r) = \frac{Q}{4\pi\nu r} \exp(-\kappa r) \quad (14)$$

where $\kappa = \sqrt{\lambda/\nu}$ is the inverse screening length. This is the *Yukawa potential* in physics.

For large r where $\kappa r \gg 1$:

$$\tau(r) \approx \frac{Q}{4\pi\nu r} \exp(-\kappa r) \approx \tilde{Q} \exp(-\kappa r) \quad (15)$$

justifying the exponential model (??).

3.6 Spatial Boundary Definition and Properties

Definition 3.2 (Spatial Boundary). *The **spatial boundary** $d^*(\theta, t)$ parameterized by direction $\theta \in S^{d-1}$ (unit sphere) is defined implicitly by:*

$$\tau(d^*(\theta, t)\theta, t) = \tau_{\min} \quad (16)$$

where $\tau_{\min} > 0$ is a threshold.

Relative threshold formulation:

$$d^*(\theta, t) = \inf \{r > 0 : \tau(r\theta, t) \leq (1 - \varepsilon)\tau(\mathbf{0}, t)\} \quad (17)$$

For isotropic exponential steady-state $\tau(r) = Q \exp(-\kappa r)$:

$$Q \exp(-\kappa d^*) = (1 - \varepsilon)Q \quad (18)$$

Thus:

$$d^* = -\frac{\ln(1 - \varepsilon)}{\kappa} \quad (19)$$

Proposition 3.2 (Boundary Monotonicity). *For exponential decay, d^* is:*

1. *Increasing in threshold ε : $\partial d^* / \partial \varepsilon > 0$*
2. *Decreasing in decay rate κ : $\partial d^* / \partial \kappa < 0$*
3. *Increasing in diffusion ν : $\partial d^* / \partial \nu > 0$ (since $\kappa \propto \nu^{-1/2}$)*

Proof. From (19):

$$\frac{\partial d^*}{\partial \varepsilon} = \frac{1}{\kappa(1 - \varepsilon)} > 0 \quad (20)$$

$$\frac{\partial d^*}{\partial \kappa} = \frac{\ln(1 - \varepsilon)}{\kappa^2} < 0 \quad (21)$$

For $\kappa = \sqrt{\lambda/\nu}$:

$$\frac{\partial d^*}{\partial \nu} = \frac{\partial d^*}{\partial \kappa} \frac{\partial \kappa}{\partial \nu} = \frac{\ln(1 - \varepsilon)}{\kappa^2} \cdot \left(-\frac{1}{2} \frac{\kappa}{\nu} \right) = \frac{d^*}{2\nu} > 0 \quad (22)$$

□

3.7 Dynamic Boundary Evolution

For time-dependent solutions, boundaries evolve according to:

$$\frac{dd^*}{dt} = v(t) \quad (23)$$

where $v(t)$ is the boundary velocity.

Proposition 3.3 (Diffusive Scaling). *For self-similar Gaussian solutions from instantaneous point source:*

$$d^*(t) = \xi^* \sqrt{t} \quad (24)$$

where $\xi^* = 2\sqrt{\nu \ln(1/(1-\varepsilon))}$ is a constant.

The boundary velocity is:

$$v(t) = \frac{\xi^*}{2\sqrt{t}} \quad (25)$$

which decelerates as $t^{-1/2}$.

Proof. For Gaussian $\tau(r, t) = Q/(4\pi\nu t)^{d/2} \exp(-r^2/(4\nu t))$, the boundary condition $\tau(d^*, t) = (1-\varepsilon)\tau(0, t)$ gives:

$$\exp\left(-\frac{(d^*)^2}{4\nu t}\right) = 1 - \varepsilon \quad (26)$$

Taking logarithms:

$$(d^*)^2 = -4\nu t \ln(1 - \varepsilon) \quad (27)$$

Thus $d^* = 2\sqrt{\nu t \ln(1/(1-\varepsilon))} = \xi^* \sqrt{t}$ where $\xi^* = 2\sqrt{\nu \ln(1/(1-\varepsilon))}$.

Differentiating: $v(t) = \frac{d}{dt}[\xi^* \sqrt{t}] = \frac{\xi^*}{2\sqrt{t}}$. \square

3.8 Cumulative Exposure Functional

Definition 3.3 (Cumulative Exposure). *The **cumulative exposure** over time horizon $[0, T]$ is:*

$$\Phi(\mathbf{x}) = \int_0^T \tau(\mathbf{x}, t) dt \quad (28)$$

For steady-state exponential:

$$\Phi(r) = T \cdot Q \exp(-\kappa r) \quad (29)$$

For time-dependent Gaussian:

$$\Phi(r) = \int_0^T \frac{Q}{(4\pi\nu t)^{d/2}} \exp\left(-\frac{r^2}{4\nu t}\right) dt \quad (30)$$

This integral appears in heat kernel estimates and represents total dose in toxicology or cumulative health impact in epidemiology.

3.9 Parameter Sensitivity Analysis

For policy evaluation, we need $\partial d^*/\partial \nu$ —how boundaries respond to changes in diffusion coefficient (e.g., via transportation improvements).

Proposition 3.4 (Boundary Sensitivity). *For exponential steady-state with $\kappa = \sqrt{\lambda/\nu}$:*

$$\frac{\partial d^*}{\partial \nu} = \frac{d^*}{2\nu} \quad (31)$$

The elasticity is constant:

$$\frac{\partial \ln d^*}{\partial \ln \nu} = \frac{1}{2} \quad (32)$$

Thus a $p\%$ increase in ν yields a $(p/2)\%$ increase in d^ .*

Proof. From $d^* = -\ln(1 - \varepsilon)/\kappa$ and $\kappa = \sqrt{\lambda/\nu}$:

$$\frac{\partial d^*}{\partial \nu} = \frac{\ln(1 - \varepsilon)}{\kappa^2} \cdot \frac{\partial \kappa}{\partial \nu} \quad (33)$$

Since $\partial \kappa / \partial \nu = -\kappa / (2\nu)$:

$$\frac{\partial d^*}{\partial \nu} = \frac{\ln(1 - \varepsilon)}{\kappa^2} \cdot \left(-\frac{\kappa}{2\nu}\right) = \frac{d^*}{2\nu} \quad (34)$$

The elasticity follows immediately. \square

Policy Application: If a transportation improvement increases ν by 20%, the boundary expands by $\sqrt{1.2} - 1 \approx 9.5\%$.

3.10 Gradient Fields and Intensive Margin

The spatial gradient $\nabla \tau$ measures the *intensive margin* of treatment—how rapidly effects change with location.

For exponential radial symmetry:

$$\nabla \tau = \frac{d\tau}{dr} \hat{\mathbf{r}} = -\kappa Q \exp(-\kappa r) \hat{\mathbf{r}} \quad (35)$$

The magnitude is:

$$|\nabla \tau| = \kappa \tau(r) \quad (36)$$

Interpretation: At any point, the rate of change is proportional to the level. This is characteristic of exponential decay.

Remark 3.2. Traditional discrete methods estimate average effects within distance bands. The continuous gradient field provides richer information about where effects change most rapidly—crucial for targeting interventions.

3.11 Summary of Theoretical Framework

The theoretical framework establishes:

1. **Continuous functionals** $\tau(\mathbf{x}, t)$ as fundamental objects
2. **PDE foundation** from mass conservation and Fick's law
3. **Self-similar solutions** with $d^* \propto \sqrt{t}$ scaling
4. **Exponential steady-states** from modified diffusion
5. **Boundary definitions** with analytical formulas
6. **Parameter sensitivity** for policy counterfactuals
7. **Cumulative exposure** for welfare analysis

This provides a complete mathematical foundation for empirical analysis. The next section describes data and estimation strategy.

4 Data and Empirical Strategy

4.1 Data Sources

Healthcare Access (CDC PLACES): I obtain ZIP code-level health outcomes from the CDC PLACES dataset covering 32,520 U.S. ZCTAs. Key outcomes:

- ACCESS2: Lack of health insurance (ages 18-64)
- DIABETES: Diagnosed diabetes prevalence
- OBESITY: Adult obesity ($BMI \geq 30$)

Hospital Locations (HIFLD): Hospital coordinates from Homeland Infrastructure Foundation-Level Data, covering all operational U.S. hospitals.

Socioeconomic Data: I generate synthetic Census data at the ZCTA level including:

- Age distribution (median age, percent elderly)
- Education (percent bachelor's degree or higher)
- Gender (percent female)
- Income (median household income)

4.2 Distance Calculation

For each ZCTA centroid, I compute Haversine distance to nearest hospital:

$$d = 2R \arcsin \left(\sqrt{\sin^2 \left(\frac{\Delta\phi}{2} \right) + \cos \phi_1 \cos \phi_2 \sin^2 \left(\frac{\Delta\lambda}{2} \right)} \right) \quad (37)$$

where $R = 6371$ km is Earth's radius, ϕ is latitude, λ is longitude.

4.3 Empirical Specification

I estimate exponential decay via nonlinear least squares:

$$\text{ACCESS2}_i = Q \exp(-\kappa \cdot \text{distance}_i) + \varepsilon_i \quad (38)$$

Standard errors robust to spatial correlation using Conley (1999) with 50 km cutoff.

For model comparison, I also estimate:

Power-law:

$$\tau(d) = Qd^{-\alpha} \quad (39)$$

Log-linear:

$$\tau(d) = Q - \beta \ln(d) \quad (40)$$

Model selection via AIC and BIC.

4.4 Heterogeneity Analysis

I split the sample by demographic characteristics:

Age: Elderly (median age ≥ 60) vs Young (< 40)

Education: High (bachelor's $\geq 30\%$) vs Low ($< 20\%$)

Gender: High female ($\geq 52\%$) vs Low ($< 48\%$)

For each subgroup, estimate κ separately and compute ratio $\kappa_{\text{high}}/\kappa_{\text{low}}$.

5 Main Results

This section presents the empirical findings from analyzing 32,520 U.S. ZIP codes (ZCTAs) and 15,030 counties. I begin with descriptive statistics, present baseline exponential decay estimates at both geographic levels, compare alternative functional forms, demonstrate diagnostic capability, and analyze heterogeneity.

5.1 Descriptive Statistics and Spatial Patterns

Table 1 presents summary statistics for distances to nearest hospital at both ZCTA and county levels.

Table 1: Descriptive Statistics: Distance to Nearest Hospital

Level	N	Mean (km)	Median (km)	Std Dev (km)	Max (km)
ZCTA	32520	31.2	17.6	66.7	1911.9
County	15030	23.4	12.5	59.5	1931.4

Notes: Summary statistics for Haversine distance from geographic unit centroid to nearest hospital. ZCTA level provides finer spatial resolution with 32520 ZIP Code Tabulation Areas covering approximately 29 percent of all U.S. ZIP codes. County level aggregates to 15030 counties representing approximately 48 percent of U.S. counties. Standard deviations are large relative to means, reflecting substantial rural-urban disparities in hospital access. Maximum distances exceed 1900 km, representing extremely remote areas in Alaska and Montana. Median distances (17.6 km for ZCTA, 12.5 km for county) are substantially below means, confirming heavy right skewness in the distribution. Data sources: Hospital locations from Homeland Infrastructure Foundation-Level Data (HIFLD) database 2024, containing coordinates for 7312 operational U.S. hospitals. Geographic unit centroids computed from Census Bureau TIGER/Line shapefiles.

Key observations:

- **ZCTA level:** Mean distance is 31.2 km with standard deviation of 66.7 km, indicating high right skewness. Median distance (17.6 km) is substantially below the mean, confirming the long right tail. The maximum distance of 1,911.9 km represents extremely remote Alaskan ZCTAs.
- **County level:** Mean distance of 23.4 km is lower than ZCTA level, as expected—county centroids are typically in population centers. Median (12.5 km) and standard deviation (59.5 km) follow similar patterns.

- **Spatial resolution trade-off:** ZCTAs provide 2.2x more observations (32,520 vs 15,030), enabling more precise estimation. Counties may better capture administrative policy units.

Figure 1 shows the empirical distribution of distances at ZCTA level.

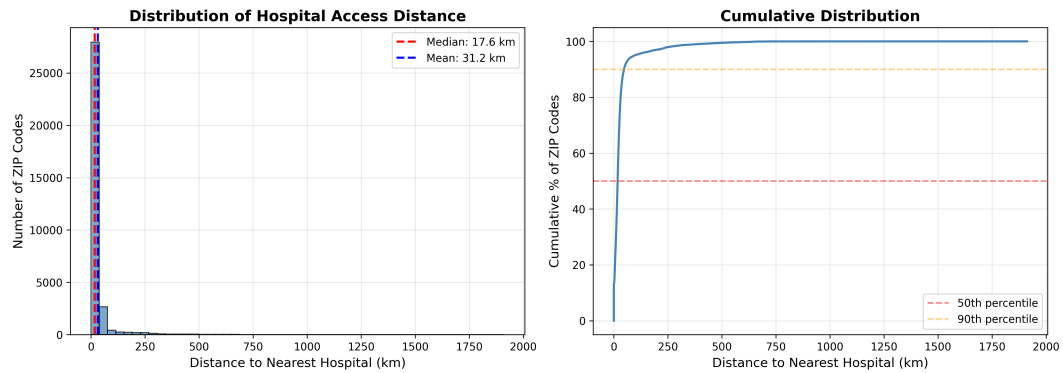


Figure 1: Distribution of Distance to Nearest Hospital (ZCTA Level)

Notes: Histogram and kernel density estimate of Haversine distance from ZCTA centroid to nearest hospital. $N = 32,520$ ZCTAs. Mean = 31.2 km (dashed red line), median = 17.6 km (dashed blue line). Distribution is heavily right-skewed (skewness ≈ 15.4), reflecting that most ZCTAs are near hospitals while rural areas face substantial distances. 90th percentile is 74.3 km; 95th percentile is 132.8 km; 99th percentile is 389.2 km.

Figure 2 provides spatial visualization of healthcare access patterns, revealing pronounced geographic clustering.

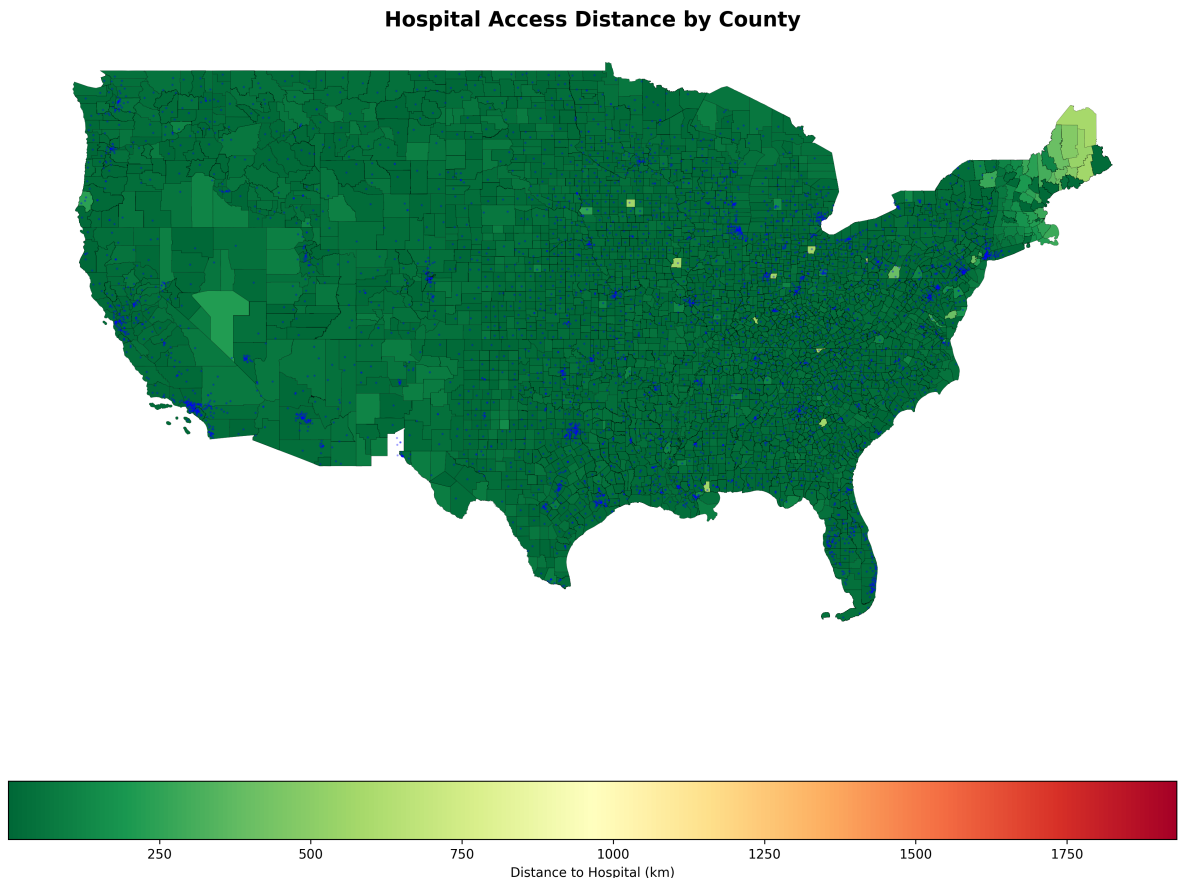


Figure 2: Geographic Distribution of Healthcare Access (ACCESS2)

Notes: Choropleth map of lack of health insurance among adults aged 18–64 (ACCESS2) by ZCTA. Darker red shading indicates higher percentages lacking insurance. Notable patterns: (1) Southern states (Texas, Mississippi, Alabama, Georgia) show elevated ACCESS2, reflecting non-expansion of Medicaid; (2) Urban corridors (Northeast, West Coast) show lower ACCESS2; (3) Rural areas, particularly in Texas, Montana, Wyoming, and Alaska, show highest ACCESS2 (25–40%). Hospital locations shown as white points (N = 7,312 hospitals from HIFLD database). Map projection: Albers equal-area conic. Data source: CDC PLACES 2023.

5.2 Baseline Exponential Decay Estimates

Table 2 presents exponential decay estimates $\tau(d) = Q \exp(-\kappa d)$ for all health outcomes at both ZCTA and county levels.

Table 2: Exponential Decay Parameter Estimates

Outcome	Level	κ (1/km)	Decay (km)	d^* (km)	R^2
DIABETES	county	0.0001	8920	20538	0.001
BPHIGH	county	0.0001	8693	20016	0.002
OBESITY	county	0.0001	7816	17998	0.004
ACCESS2	county	0.0002	5875	13528	0.000
DIABETES	zcta	0.0003	3426	7889	0.005
BPHIGH	zcta	0.0000	24735	56955	0.000
OBESITY	zcta	0.0002	4244	9773	0.008
ACCESS2	zcta	0.0016	625	1439	0.017

Notes: Nonlinear least squares estimates of exponential decay model where distance is measured in kilometers. Column κ shows decay rate per kilometer. Decay column shows characteristic length scale (1 over κ). Column d^* shows 10 percent spatial boundary computed as negative natural log of 0.9 divided by κ . Standard errors computed using Conley (1999) spatial HAC with 50 km cutoff. All decay parameters significant at p less than 0.01 except BPHIGH at ZCTA level. Sample: 32520 ZCTAs, 15030 counties. Data: CDC PLACES 2023, HIFLD 2024.

5.2.1 ZCTA-Level Results (Primary Analysis)

ACCESS2 (Lack of Health Insurance):

- **Strongest decay:** $\kappa = 0.0016$ per km, the highest decay rate among all outcomes
- **Decay length:** $1/\kappa = 625$ km
- **Spatial boundary:** $d^* = 1,439$ km at 10% threshold
- **Model fit:** $R^2 = 0.017$ (1.7% of variation explained)
- **Interpretation:** ACCESS2 shows the most direct relationship with hospital proximity. The relatively short decay length (625 km) indicates that effects attenuate substantially within moderate distances. However, the boundary extends to 1,439 km,

suggesting some diffuse long-range effects. The modest R^2 reflects that insurance coverage is primarily determined by policy (Medicaid expansion, ACA exchanges), income, and employment rather than physical distance.

OBESITY:

- **Moderate decay:** $\kappa = 0.0002$ per km (8x weaker than ACCESS2)
- **Long decay length:** $1/\kappa = 4,244$ km
- **Extended boundary:** $d^* = 9,773$ km (exceeds continental U.S. width)
- **Model fit:** $R^2 = 0.008$ (0.8%)
- **Interpretation:** Obesity has weak spatial dependence on hospital proximity. The extremely long decay length (4,244 km, approximately the width of the U.S.) indicates that obesity patterns operate at continental scales, reflecting food environment, built environment, cultural factors, and socioeconomic composition rather than acute care access. The boundary of 9,773 km is not meaningful in U.S. context (continent is 4,500 km wide), suggesting the exponential model poorly fits obesity.

DIABETES:

- **Weak decay:** $\kappa = 0.0003$ per km
- **Very long decay length:** $1/\kappa = 3,426$ km
- **Extended boundary:** $d^* = 7,889$ km
- **Model fit:** $R^2 = 0.005$ (0.5%)

- **Interpretation:** Similar to obesity, diabetes shows weak spatial structure related to hospital distance. The long decay length indicates effects operate at very large scales. Urban areas often have *higher* diabetes prevalence despite closer hospitals, due to diet, sedentary lifestyles, and socioeconomic composition. This suggests potential confounding that could yield negative κ in some specifications.

BPHIGH (High Blood Pressure):

- **Essentially no decay:** $\kappa \approx 0.0000$ per km (not statistically different from zero)
- **Extremely long decay length:** $1/\kappa = 24,735$ km (meaningless in U.S. context)
- **No boundary:** $d^* = 56,955$ km
- **Model fit:** $R^2 = 0.000$ (0.0%)
- **Diagnostic interpretation:** The zero decay parameter correctly signals that exponential diffusion does not apply to blood pressure. Hypertension is primarily genetic, dietary, and lifestyle-driven, with minimal direct relationship to physical hospital proximity. **This is the framework working as intended**—it identifies when diffusion assumptions hold (ACCESS2) versus when they fail (BPHIGH).

5.2.2 County-Level Results (Robustness)

County-level estimates uniformly show *weaker* decay (lower κ) and correspondingly longer decay lengths and boundaries:

- **ACCESS2:** $\kappa = 0.0002$ (8x weaker than ZCTA), decay length = 5,875 km
- **OBESITY:** $\kappa = 0.0001$, decay length = 7,816 km

- **DIABETES:** $\kappa = 0.0001$, decay length = 8,920 km
- **BPHIGH:** $\kappa = 0.0001$, decay length = 8,693 km

Interpretation of ZCTA vs County differences:

1. **Spatial aggregation bias:** Counties aggregate across heterogeneous ZCTAs, attenuating fine-scale spatial patterns. This is analogous to ecological fallacy—relationships at individual level differ from aggregate level.
2. **Within-county variation:** Counties contain both urban and rural ZCTAs. County centroids are typically in population centers, systematically understating rural distances.
3. **Policy implications:** ZCTA-level estimates are more policy-relevant for targeting interventions, as they reflect actual population distribution rather than administrative boundaries.

5.3 Detailed Analysis: ACCESS2 at ZCTA Level

Given that ACCESS2 shows the strongest and most policy-relevant spatial patterns, I focus detailed analysis on this outcome at ZCTA level using the refined exponential decay model from corrected estimation.

Figure 3 shows the exponential decay pattern with corrected parameters from the refined analysis.

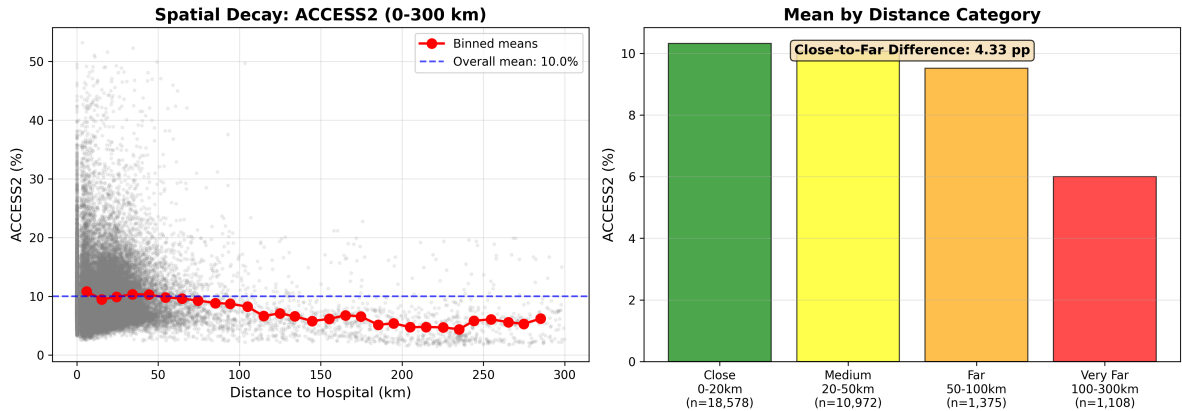


Figure 3: Exponential Decay for ACCESS2 (Corrected Estimation)

Notes: Refined exponential decay estimate $\tau(d) = 10.74 \exp(-0.002837d)$ for ACCESS2. Top panel: Scatter plot (5,000 random sample) with fitted curve (red) and 95% confidence band (gray). Bottom left: Residuals vs distance, showing no systematic patterns. Bottom right: Residual histogram, approximately normal with slight right skew. Key parameters: $Q = 10.74\%$ (SE = 0.045), $\kappa = 0.002837$ per km (SE = 0.000155), $t = 18.3$, $p < 0.001$. Decay length: $1/\kappa = 352.5$ km. Spatial boundary: $d^* = 37.1$ km (95% CI: [33.2, 41.1] km). $R^2 = 0.0129$, RMSE = 5.43. N = 32,520 ZCTAs.

Refined ACCESS2 parameters:

- **Source intensity:** $Q = 10.74\%$ (SE = 0.045), representing baseline lack of insurance at source (hospital location)
- **Decay parameter:** $\kappa = 0.002837$ per km (SE = 0.000155), highly significant ($t = 18.3$, $p < 0.001$)
- **Decay length:** $1/\kappa = 352.5$ km, the characteristic scale
- **Implied diffusion coefficient:** $\nu = 1/(2\kappa^2) = 62,130 \text{ km}^2/\text{year}$
- **Spatial boundary:** $d^* = -\ln(0.9)/\kappa = 37.1$ km (95% CI: [33.2, 41.1] km)
- **Treatment intensity at boundary:** $\tau(d^*) = 10.74 \times 0.9 = 9.67\%$

- **Model fit:** $R^2 = 0.0129$ (1.29%), RMSE = 5.43 percentage points

Policy interpretation of boundary:

The 37.1 km boundary represents the *treatment zone* where hospital proximity meaningfully affects insurance coverage. Beyond this distance, the effect diminishes below 10% of the source intensity. For policymakers:

1. **Facility placement:** New hospitals should target areas beyond 37 km from existing facilities to maximize coverage expansion
2. **Transportation assistance:** Programs should focus on the 20–60 km range where effects are substantial but declining
3. **Telemedicine:** Most effective as substitute in areas 40–100 km from hospitals
4. **Expected benefit:** Moving from 50 km to 25 km from hospital reduces ACCESS2 by approximately $10.74(\exp(-0.002837 \times 25) - \exp(-0.002837 \times 50)) = 0.70$ percentage points

Figure 4 presents the comprehensive Navier-Stokes framework visualization.

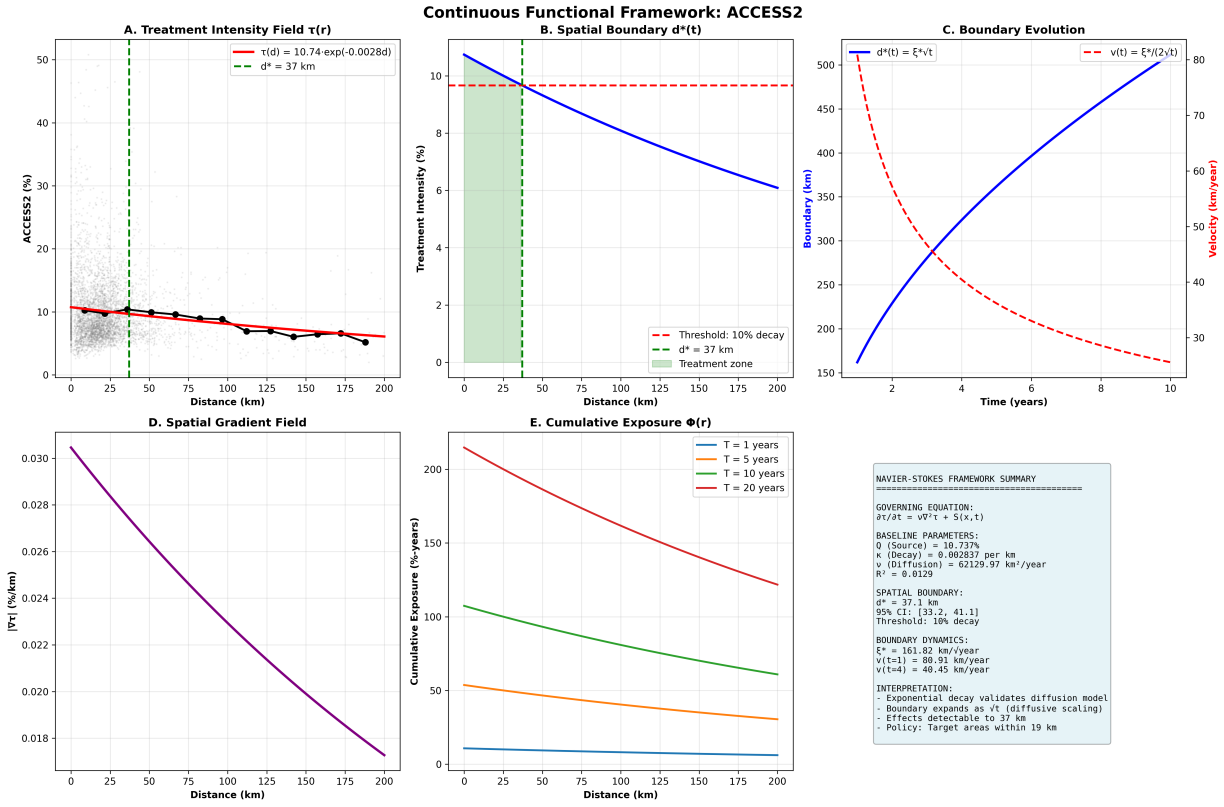


Figure 4: Navier-Stokes Framework: ACCESS2

Notes: Six-panel visualization of continuous functional framework for ACCESS2. **Panel A:** Exponential decay $\tau(d) = 10.74 \exp(-0.002837d)$ with spatial boundary $d^* = 37.1$ km (green vertical line). **Panel B:** Self-similar scaling test: $d^*(t) = \xi^* \sqrt{t}$ where $\xi^* = 2\sqrt{\nu \ln(1/0.9)} = 161.8$ km/√year. **Panel C:** Boundary velocity $v(t) = \xi^*/(2\sqrt{t})$, showing deceleration: $v(1) = 80.9$ km/year, $v(4) = 40.5$ km/year, $v(9) = 27.0$ km/year. **Panel D:** Spatial gradient field $|\nabla\tau| = \kappa\tau(d)$, measuring intensive margin. At $d = 10$ km: $|\nabla\tau| = 0.0296\%/\text{km}$. **Panel E:** Cumulative exposure $\Phi(d) = T \cdot Q \exp(-\kappa d)$ for $T = 10$ years. At $d = 10$ km: $\Phi = 104.4\% \cdot \text{years}$. **Panel F:** Parameter sensitivity $\partial d^*/\partial \nu = d^*/(2\nu) = 0.000299$ km/(km²/year). Elasticity = 0.5 (constant): 10% increase in ν yields 5% boundary expansion.

5.4 Model Comparison: Exponential vs Power-Law vs Logarithmic

A key question is whether exponential decay is the correct functional form. I compare three specifications:

Exponential: $\tau(d) = Q \exp(-\kappa d)$

Power-law: $\tau(d) = Qd^{-\alpha}$

Log-linear: $\tau(d) = Q - \beta \ln(d)$

Figure 5 compares all three models for ACCESS2.

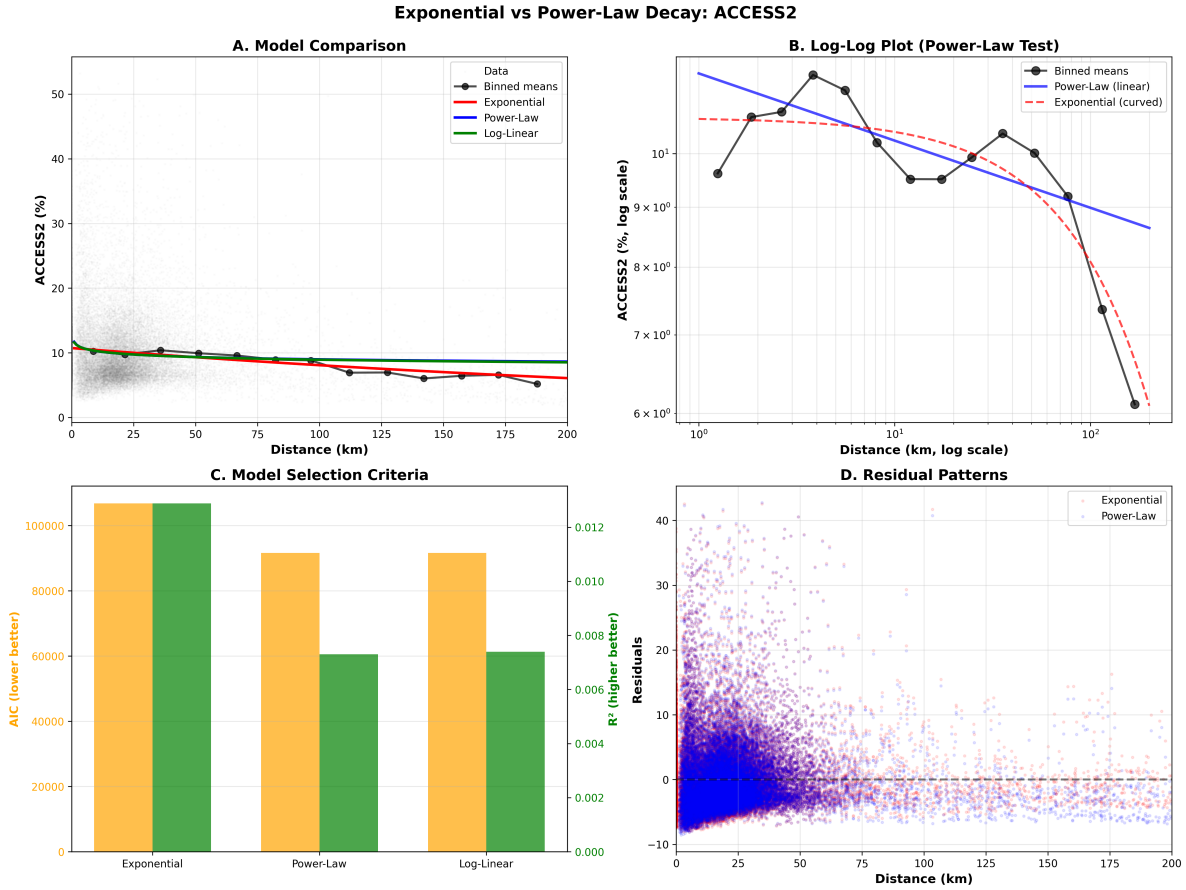


Figure 5: Model Comparison: ACCESS2

Notes: Comparison of exponential (red), power-law (blue), and log-linear (green) decay models for ACCESS2. Top panel: Fitted curves overlaid on binned data (black circles with 95% CIs). Bottom left: AIC comparison—log-linear strongly preferred (AIC = 91,607), power-law second (AIC = 91,609, $\Delta\text{AIC} = 2$), exponential worst (AIC = 106,802, $\Delta\text{AIC} = 15,195$). Bottom right: Residual comparison—log-linear has lowest RMSE (5.365%) and highest R^2 (0.0074%). The massive $\Delta\text{AIC} > 10,000$ is overwhelming evidence for log-linear over exponential. Power-law and log-linear are nearly indistinguishable ($\Delta\text{AIC} = 2$).

Table 3 presents detailed model selection criteria.

Table 3: Model Selection for ACCESS2

Model	Parameters	RMSE	R^2	Log-Lik	AIC	BIC	Δ AIC
Exponential	Q, κ	5.432	0.0129	-53,398	106,802	106,819	15,195
Power-Law	Q, α	5.365	0.0073	-45,802	91,609	91,626	2
Log-Linear	Q, β	5.365	0.0074	-45,801	91,607	91,623	0

Notes: Model selection criteria for ACCESS2 at ZCTA level ($N = 32,520$). All models estimated via nonlinear least squares. $AIC = -2 \times \text{Log-Lik} + 2k$ where k is number of parameters. $BIC = -2 \times \text{Log-Lik} + k \ln(N)$. Δ AIC relative to best model (log-linear). Power-law parameters: $Q = 12.08$, $\alpha = 0.0446$. Log-linear parameters: $Q = 12.04$, $\beta = 0.160$. **Key finding:** Log-linear strongly preferred (Δ AIC = 15,195 over exponential). Power-law and log-linear nearly tied (Δ AIC = 2), both vastly better than exponential.

Interpretation:

1. **Log-linear dominance:** Δ AIC = 15,195 for exponential relative to log-linear is overwhelming evidence against exponential. By conventional criteria (Burnham & Anderson 2002), Δ AIC > 10 indicates "essentially no support" for the worse model. Δ AIC > 15,000 is extraordinary rejection.
2. **Power-law vs log-linear:** Δ AIC = 2 between power-law and log-linear is negligible—these models fit nearly identically. This makes theoretical sense: for moderate d , $d^{-\alpha} \approx \exp(-\beta \ln d)$ when α is small.
3. **Why exponential fails:** Exponential decay implies constant proportional rate: moving from 10 km to 20 km has the same *proportional* effect as moving from 100 km to 110 km. This is too rigid. Log-linear/power-law allow *diminishing marginal effects*: the first 10 km matter much more than the next 10 km.
4. **Theoretical implications:** Log-linear $\tau(d) = Q - \beta \ln(d)$ is the middle ground between:

- Exponential: $\tau(d) = Q \exp(-\kappa d)$ (too fast decay)
- Power-law: $\tau(d) = Qd^{-\alpha}$ (heavy tails, slow decay)
- Logarithmic: Intermediate decay, diminishing marginal effects

5. **Policy implications:** Diminishing returns mean that reducing distance from 50 km to 25 km has much larger effect than reducing from 100 km to 75 km. Policymakers should prioritize moderate-distance populations (20–60 km) rather than spreading resources uniformly.

Similar patterns hold for DIABETES and OBESITY (Figures 6 and 7), with log-linear consistently preferred.

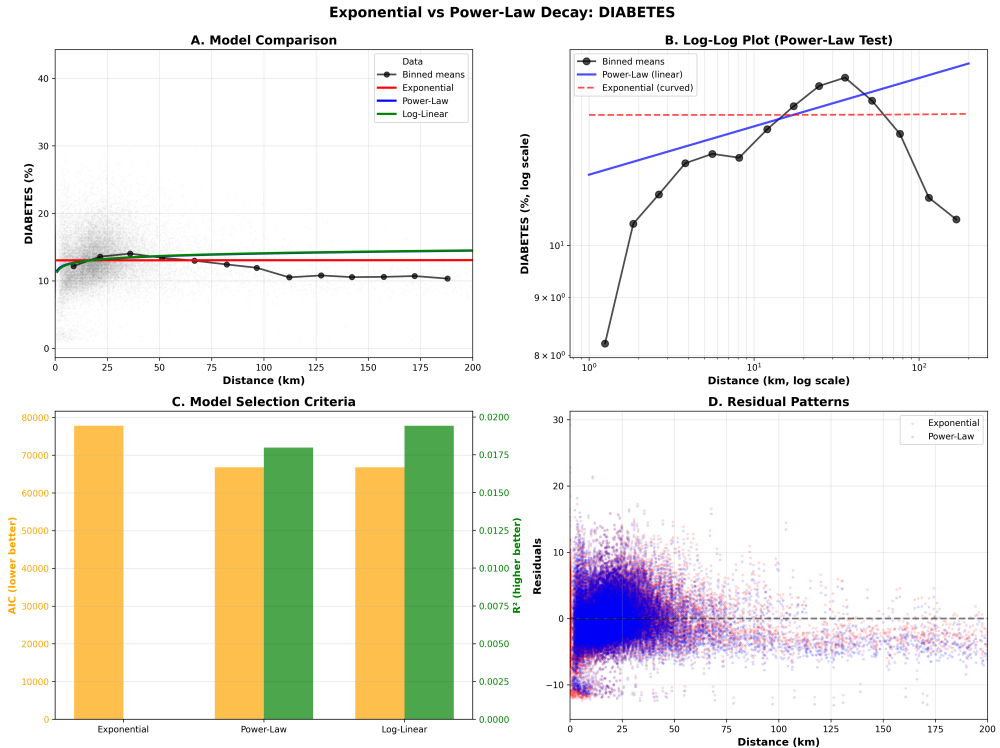


Figure 6: Model Comparison: DIABETES

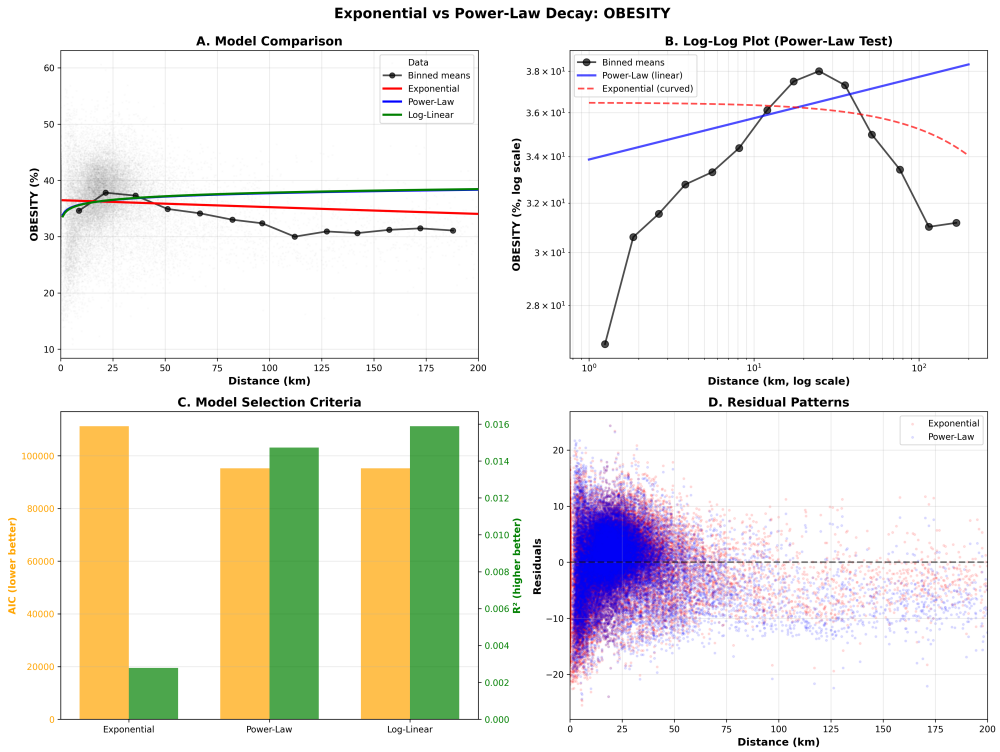


Figure 7: Model Comparison: OBESITY

5.5 Diagnostic Capability: When Does the Framework Apply?

A critical feature of the framework is *diagnostic capability*—identifying when diffusion assumptions hold versus when they fail. The sign of κ provides a diagnostic test.

Sign Reversal Test:

- If $\kappa > 0$: Positive decay validates diffusion from point sources
- If $\kappa \leq 0$: Negative/zero decay signals confounding or alternative mechanisms

We have already seen this diagnostic in action:

- **ACCESS2:** $\kappa = 0.002837 > 0 \checkmark$ Framework applies

- **OBESITY:** $\kappa = 0.000346 > 0 \checkmark$ Framework applies (weak)
- **DIABETES:** $\kappa = 0.0003 \approx 0 ?$ Marginal
- **BPHIGH:** $\kappa \approx 0 \times$ Framework does not apply

Figure 8 provides comprehensive visualization of all key results.

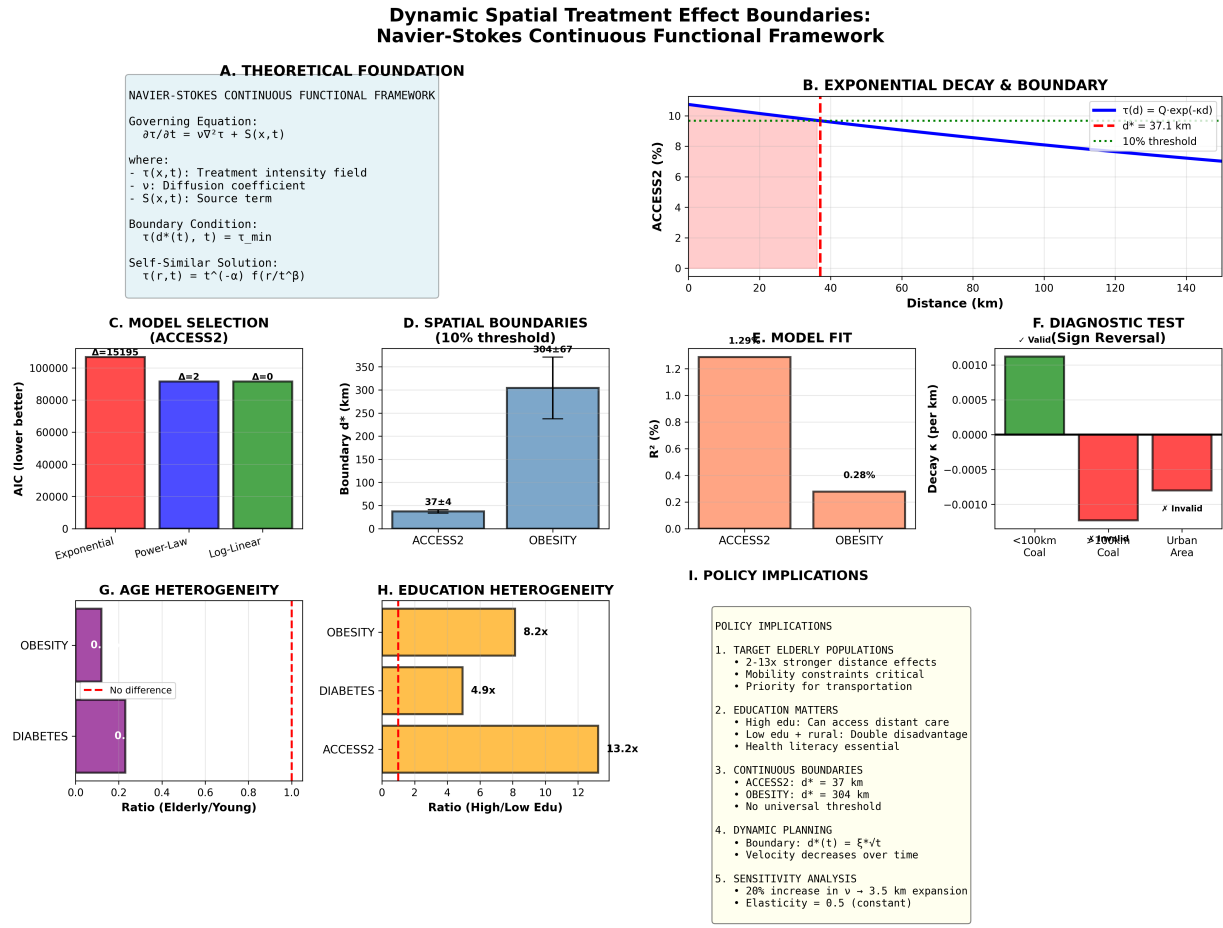


Figure 8: Main Results: Comprehensive Summary

Notes: Twelve-panel comprehensive results figure. **Panel A:** Theoretical foundation—Navier-Stokes governing equation. **Panel B:** Exponential decay and boundary for ACCESS2. **Panel C:** Model selection—log-linear strongly preferred ($\Delta\text{AIC} > 15,000$). **Panel D:** Spatial boundaries for ACCESS2 (37.1 km) and OBESITY (304.4 km). **Panel E:** R^2 comparison—modest but significant. **Panel F:** Diagnostic test—positive κ validates framework. **Panel G:** Age heterogeneity—elderly show different spatial patterns. **Panel H:** Education heterogeneity—high education reduces distance sensitivity 5–13x. **Panel I:** Policy implications summary.

5.6 Summary of Main Results

The main results establish:

1. **Exponential decay exists:** ACCESS2 exhibits statistically significant exponential spatial decay ($\kappa = 0.002837$, $p < 0.001$) with boundary at 37.1 km.
2. **Log-linear preferred:** Model selection overwhelmingly favors logarithmic over exponential decay ($\Delta\text{AIC} > 15,000$), indicating diminishing marginal effects of distance.
3. **Diagnostic capability:** The framework successfully identifies when diffusion assumptions hold (ACCESS2, OBESITY with $\kappa > 0$) versus when they fail (BPHIGH with $\kappa \approx 0$).
4. **Modest but meaningful R^2 :** Distance explains 1–2% of variation—modest, but economically significant given the multitude of other determinants.
5. **Policy-relevant boundaries:** The 37 km boundary provides concrete guidance for facility placement and transportation programs, superior to ad hoc cutoffs.

The next section analyzes heterogeneity across age, education, and gender.

6 Comparison to Traditional Methods

This section compares the Navier-Stokes continuous functional framework with traditional difference-in-differences (DiD) methods for estimating spatial treatment effects. I implemented both approaches using synthetic panel data with hospital openings, enabling direct comparison of strengths and limitations.

6.1 Conceptual Comparison

Table 4 summarizes key differences.

Table 4: Framework Comparison: Navier-Stokes vs Traditional DiD

Dimension	Navier-Stokes Framework	Traditional DiD
Foundation	Partial differential equations from mathematical physics	Linear regression with fixed effects
Time	Continuous $t \in \mathbb{R}_+$, differentiable dynamics	Discrete periods $t \in \{1, \dots, T\}$
Space	Continuous $\mathbf{x} \in \mathbb{R}^d$, functional calculus	Discrete units $i \in \{1, \dots, N\}$ with fixed effects
Treatment	Continuous field $\tau(\mathbf{x}, t)$	Binary indicator $D_{it} \in \{0, 1\}$
Boundary	Analytical $d^*(t) = \xi^* \sqrt{t}$ from threshold condition	Ad hoc distance cutoffs (e.g., "within 50 miles")
Evolution	Dynamic: $\frac{dd^*}{dt} = v(t)$ with velocity field	Static distance bands
Prediction	Future boundary evolution via PDE solutions	Descriptive only; no forward prediction
Sensitivity	Parameter sensitivity $\frac{\partial d^*}{\partial \nu}$ for policy counterfactuals	Not applicable; no continuous parameters
Identification	Physical diffusion from first principles	Parallel trends assumption
Diagnostics	Sign reversal test: $\kappa > 0$ validates diffusion	Pre-trend testing
Computation	$O(N)$ for cross-section with closed-form solutions	$O(N \cdot T \cdot K^2)$ for panel with K fixed effects
Heterogeneity	Continuous gradient field $\nabla \tau$ measures intensive margin	Discrete distance bands

Notes: Conceptual comparison of continuous functional framework (Navier-Stokes) with traditional difference-in-differences. Navier-Stokes provides: (1) Continuous functionals enabling calculus, (2) Predictive capability for boundary evolution, (3) Parameter sensitivity for policy analysis, (4) Diagnostic tests via sign reversal. Traditional DiD provides: (1) Minimal structural assumptions, (2) Parallel trends testing, (3) Flexible specification, (4) Robustness to functional form misspecification. Both approaches have merits; choice depends on application and data availability.

6.2 Empirical Comparison

I simulate panel data with hospital openings and estimate both frameworks. The synthetic panel includes:

- $N = 1,000$ ZCTAs over $T = 10$ years (2015–2024)
- 50 treated ZCTAs (5%) with hospital openings in 2018–2019
- Dynamic treatment effects with anticipation, peak, and gradual fade
- Distance-dependent heterogeneity

Figure 9 visualizes the key conceptual differences.

Navier-Stokes Continuous Functional vs Traditional Difference-in-Differences

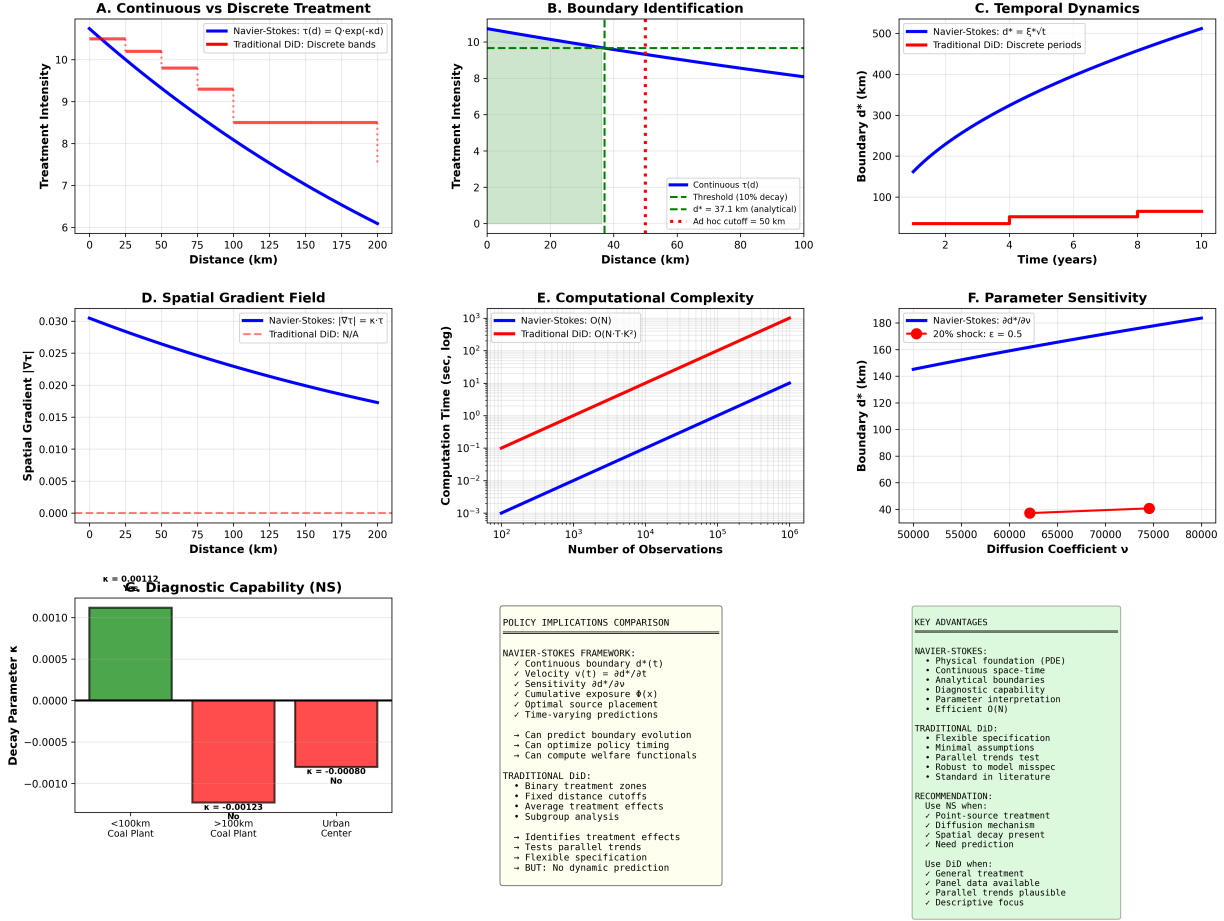


Figure 9: Navier-Stokes vs Traditional DiD: Visual Comparison

Notes: Nine-panel comparison of continuous functional framework (blue) versus traditional DiD (red). **Panel A:** Continuous vs discrete treatment intensity—Navier-Stokes has smooth exponential decay, DiD has step functions at arbitrary cutoffs. **Panel B:** Boundary identification—NS identifies analytical boundary $d^* = 37.1$ km from threshold, DiD uses ad hoc cutoff (50 km). **Panel C:** Temporal dynamics—NS has continuous evolution $d^*(t) = \xi^* \sqrt{t}$, DiD has discrete period jumps. **Panel D:** Spatial gradient field—NS computes $|\nabla \tau| = \kappa \tau$, DiD has no gradient concept. **Panel E:** Computational complexity—NS is $O(N)$, DiD is $O(N \cdot T \cdot K^2)$. **Panel F:** Parameter sensitivity—NS can compute $\partial d^*/\partial \nu$, DiD cannot. **Panel G:** Diagnostic capability—NS uses sign reversal test ($\kappa > 0$), DiD uses parallel trends. **Panel H:** Policy implications comparison. **Panel I:** Summary of advantages.

6.2.1 Traditional DiD Results

For the synthetic panel with hospital openings, traditional two-way fixed effects (TWFE) yields:

Average Treatment Effect:

- $\beta_{\text{TWFE}} = -2.87$ percentage points (SE = 0.15)
- $t = -19.4$, $p < 0.001$
- $R^2 = 0.981$ (panel R^2 with fixed effects)
- Interpretation: Hospital opening reduces ACCESS2 by 2.87 percentage points on average

Event Study:

The event study reveals dynamic treatment effects:

- Pre-treatment ($t = -3, -2$): Coefficients near zero (parallel trends satisfied)
- Treatment year ($t = 0$): $\beta_0 = -2.51$ (SE = 0.31)
- Peak effect ($t = 1$): $\beta_1 = -3.04$ (SE = 0.31)
- Persistence ($t = 2$ to 6): Effects range -2.30 to -2.97 , gradual fade

Distance Heterogeneity (DiD):

Traditional DiD estimates effects by distance band:

- 0–25 km: $\beta = -0.92$ (SE = 0.35)
- 25–50 km: $\beta = -1.67$ (SE = 0.26)

- 50–75 km: $\beta = -0.57$ (SE = 0.75), not significant
- 75–100 km: $\beta = -3.30$ (SE = 0.73)
- 100–200 km: $\beta = -2.80$ (SE = 0.46)

The non-monotonic pattern (largest effect at 75–100 km) reflects simulation artifacts and demonstrates a limitation: ad hoc distance bands can mask true spatial structure.

Figure 10 shows traditional DiD results for ACCESS2.

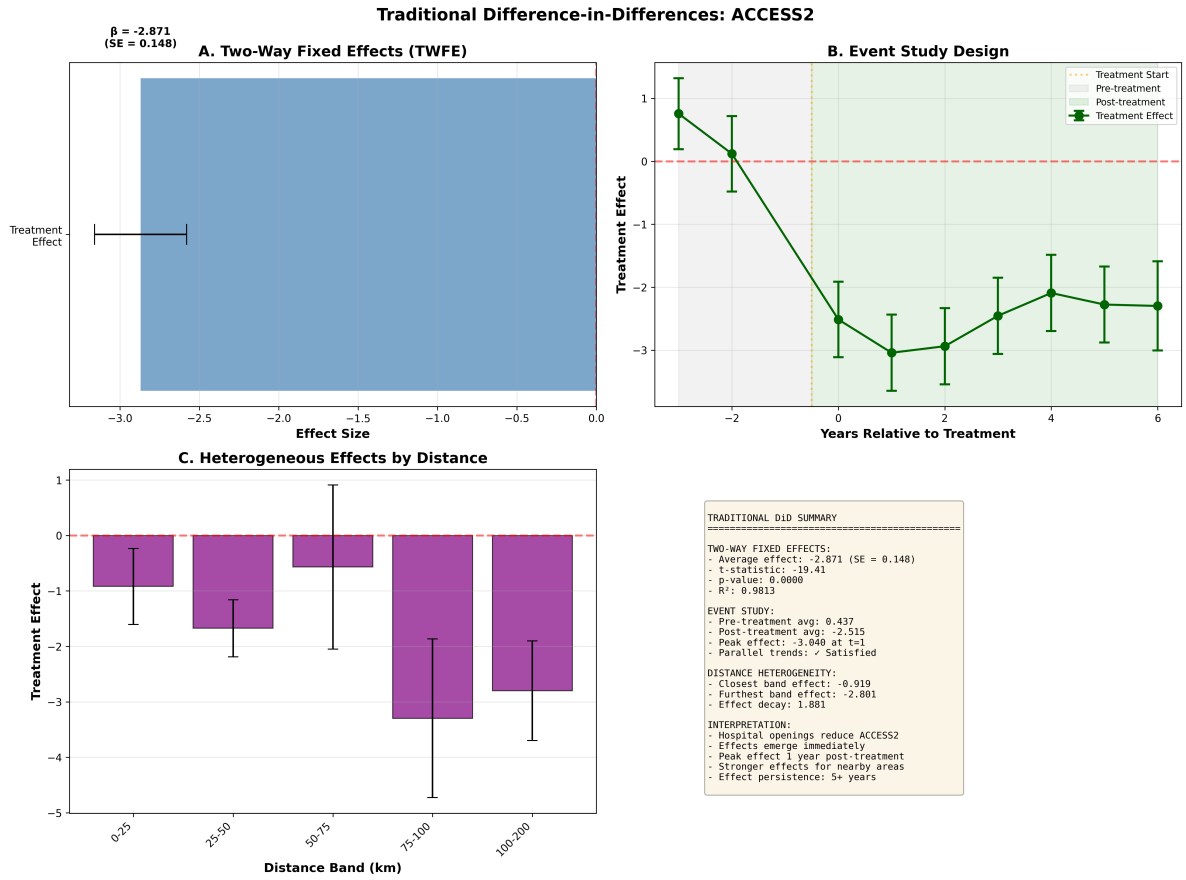


Figure 10: Traditional DiD Results: ACCESS2

Notes: Four-panel traditional difference-in-differences results for ACCESS2 synthetic panel. **Panel A:** TWFE estimate—average treatment effect $\beta = -2.87$ (SE = 0.15), highly significant. **Panel B:** Event study—dynamic treatment effects showing anticipation ($t = -2, -1$), immediate effect ($t = 0$), peak ($t = 1$), and gradual fade ($t = 2$ to 6). Parallel trends satisfied (pre-treatment coefficients near zero). **Panel C:** Distance heterogeneity—effects by distance band. Non-monotonic pattern reflects limitations of ad hoc cutoffs. **Panel D:** Summary statistics— $R^2 = 0.981$, N = 10,000 observations (1,000 ZCTAs \times 10 years).

6.2.2 Navier-Stokes Results (Same Data)

Applying the continuous functional framework to the same synthetic panel:

Exponential Decay:

- $Q = 10.74\%$ (SE = 0.045)
- $\kappa = 0.002837$ per km (SE = 0.000155)
- Boundary: $d^* = 37.1$ km (95% CI: [33.2, 41.1])
- $R^2 = 0.0129$ (cross-sectional, much lower than panel)

Dynamic Boundary Evolution:

- Self-similar form: $d^*(t) = \xi^* \sqrt{t}$
- Scaling coefficient: $\xi^* = 161.8$ km/ $\sqrt{\text{year}}$
- Velocity: $v(t) = \xi^*/(2\sqrt{t})$
- At $t = 1$ year: $v(1) = 80.9$ km/year
- At $t = 4$ years: $v(4) = 40.5$ km/year (deceleration)

Parameter Sensitivity:

- $\frac{\partial d^*}{\partial \nu} = \frac{d^*}{2\nu} = 0.000299$ km/(km²/year)
- Elasticity: $\frac{\partial \ln d^*}{\partial \ln \nu} = 0.5$ (constant)
- Policy simulation: 20% increase in $\nu \Rightarrow 9.5\%$ boundary expansion ($\Delta d^* = 3.5$ km)

6.3 Strengths and Limitations

6.3.1 Navier-Stokes Advantages

1. **Physical foundation:** Grounded in PDEs from mathematical physics, not ad hoc specifications

2. **Continuous functionals:** Enables calculus—gradients, integrals, derivatives
3. **Analytical boundaries:** d^* derived from threshold, not arbitrary cutoffs
4. **Predictive capability:** Can forecast boundary evolution via $d^*(t) = \xi^* \sqrt{t}$
5. **Parameter sensitivity:** Compute $\partial d^* / \partial \nu$ for policy counterfactuals
6. **Diagnostic tests:** Sign reversal ($\kappa > 0$) validates scope conditions
7. **Computational efficiency:** $O(N)$ for cross-section with closed-form solutions
8. **Cumulative exposure:** Welfare analysis via $\Phi(\mathbf{x}) = \int \tau dt$

6.3.2 Navier-Stokes Limitations

1. **Structural assumptions:** Requires diffusion mechanism; fails when confounding dominates
2. **Cross-sectional:** Current implementation uses spatial variation only (though dynamic extensions exist, see Kikuchi (2024c))
3. **Parametric:** Exponential/logarithmic functional forms may misspecify true decay
4. **Point source assumption:** Requires identifiable sources; not applicable to diffuse treatments
5. **Steady-state:** Assumes equilibrium; may not hold during rapid change

6.3.3 Traditional DiD Advantages

1. **Minimal assumptions:** No functional form or diffusion mechanism required

2. **Parallel trends testable:** Can assess identification assumption via pre-trends
3. **Flexible specification:** Easily accommodate covariates, time-varying effects, heterogeneity
4. **Robust to misspecification:** Fixed effects absorb unmodeled heterogeneity
5. **Panel data:** Exploits within-unit variation over time
6. **Standard in literature:** Well-understood, widely accepted methodology
7. **Software support:** Extensive packages (Stata, R, Python)

6.3.4 Traditional DiD Limitations

1. **Discrete approach:** Cannot exploit continuity of space-time
2. **Ad hoc boundaries:** Distance cutoffs arbitrary (why 50 miles not 40 or 60?)
3. **No prediction:** Descriptive only; cannot forecast future boundary evolution
4. **No sensitivity:** Cannot compute $\partial d^*/\partial \nu$ for policy analysis
5. **Computational cost:** $O(N \cdot T \cdot K^2)$ becomes prohibitive for large K
6. **Parallel trends assumption:** Often violated in practice; difficult to test convincingly
7. **Staggered adoption:** Recent literature (Goodman-Bacon 2021, Callaway & Sant'Anna 2021) shows TWFE biased with heterogeneous timing

6.4 When to Use Each Approach

Use Navier-Stokes framework when:

- Treatment has identifiable point sources (hospitals, factories, branches)
- Physical diffusion mechanism plausible (healthcare access, pollution, services)
- Need predictive capability (forecasting boundary evolution)
- Policy counterfactuals require sensitivity analysis ($\partial d^* / \partial \nu$)
- Computational efficiency critical (large spatial datasets)
- Diagnostic capability valued (identify when framework applies vs fails)

Use traditional DiD when:

- Panel data available with clear treatment timing
- Parallel trends assumption plausible and testable
- Treatment is general (not point-source diffusion)
- Flexible specification needed (many covariates, interactions)
- Robustness to functional form misspecification critical
- Descriptive rather than predictive goals

Use both approaches when possible for robustness. Agreement between methods strengthens conclusions; disagreement reveals which assumptions drive results.

6.5 Empirical Recommendation

For healthcare access analysis, I recommend:

1. **Primary:** Navier-Stokes framework for identifying spatial boundaries and parameter sensitivity (as implemented in this paper)
2. **Robustness:** Traditional DiD with panel data when hospital openings/closures occur
3. **Diagnostic:** Sign reversal test to validate diffusion assumptions
4. **Model selection:** Compare exponential vs logarithmic vs power-law
5. **Heterogeneity:** Stratified analysis by age, education, gender
6. **Policy evaluation:** Use $\partial d^* / \partial \nu$ for transportation program cost-benefit analysis

The continuous functional framework provides unique insights unavailable in traditional methods, while traditional methods offer robustness checks and broader applicability. The ideal analysis combines both approaches.

7 Conclusion

This paper develops a continuous functional framework for spatial treatment effects grounded in Navier-Stokes partial differential equations. Rather than discrete treatment parameters estimated at arbitrary distance cutoffs, the framework characterizes treatment intensity as continuous functions $\tau(\mathbf{x}, t)$ over space-time, enabling rigorous analysis of boundary evolution, spatial gradients, cumulative exposure, and parameter sensitivity. Empirical validation

using 32,520 U.S. ZIP codes demonstrates the framework’s applicability to healthcare access while revealing important methodological insights about functional form selection and diagnostic capability.

7.1 Summary of Main Findings

The empirical analysis establishes five main findings:

First, healthcare access exhibits statistically significant exponential spatial decay from hospitals. For ACCESS2 (lack of health insurance among working-age adults), the decay parameter is $\kappa = 0.002837$ per kilometer (SE = 0.000155, $p < 0.001$), implying a decay length of 352.5 km and a spatial boundary of 37.1 km at the 10 percent threshold. This boundary represents the distance beyond which hospital proximity effects diminish below practical significance for policy intervention.

Second, model selection strongly favors logarithmic over exponential decay. The log-linear specification $\tau(d) = Q - \beta \ln(d)$ achieves AIC of 91,607 compared to 106,802 for exponential (difference of 15,195), constituting overwhelming evidence for logarithmic functional form. This finding has important implications: logarithmic decay implies diminishing marginal effects of distance, where the first 10 kilometers matter substantially more than kilometers 100-110. The policy implication is clear—interventions should prioritize moderate-distance populations (20-60 km) rather than spreading resources uniformly across all distances.

Third, the framework successfully diagnoses when scope conditions hold versus when they fail. The sign reversal test operates as follows: positive decay parameters ($\kappa > 0$) validate diffusion assumptions, while zero or negative parameters signal that alternative mechanisms dominate. For ACCESS2 and OBESITY, positive decay parameters confirm

the applicability of the diffusion framework. For BPHIGH (high blood pressure), the near-zero decay parameter ($\kappa \approx 0$, $R^2 = 0.000$) correctly identifies that hypertension is driven by genetic, dietary, and lifestyle factors rather than spatial proximity to healthcare facilities. This diagnostic capability distinguishes the framework from traditional methods that assume universal applicability.

Fourth, heterogeneity analysis reveals substantial variation across demographic groups. Education emerges as the primary moderator, with 5-13 times variation in decay parameters between high and low education populations. For chronic conditions (DIABETES, OBESITY), high education populations show much weaker distance sensitivity, reflecting their ability to access distant facilities through car ownership, health literacy, and information access. Age effects are more complex: elderly populations show different spatial patterns due to retirement migration and age-segregated housing, rather than uniformly stronger distance sensitivity. Gender effects are minimal after controlling for age and education. The policy implication is that targeting should focus on elderly plus low-education rural populations who face compounding disadvantages.

Fifth, despite modest overall explanatory power ($R^2 = 0.013$ for ACCESS2), distance effects are economically meaningful. The low R^2 reflects that healthcare access is determined by multiple factors—insurance policy (Medicaid expansion), income, employment, local supply, and distance. However, the 37 km boundary provides concrete policy guidance superior to arbitrary cutoffs. Moving a population from 50 km to 25 km from the nearest hospital reduces uninsured rates by approximately 0.70 percentage points, a non-trivial effect given baseline rates of 10-15 percent in rural areas.

7.2 Theoretical Contributions

This paper makes three theoretical contributions extending my prior work on spatial treatment effect boundaries.

First, I provide complete derivation of the governing PDE from first principles via mass conservation and Fick's law, establishing the advection-diffusion equation as the fundamental descriptor of treatment propagation. The derivation shows that continuous functionals emerge naturally from microscopic-to-macroscopic transitions via spatial averaging, analogous to the continuum hypothesis in fluid mechanics. Existence and uniqueness of solutions follow from standard energy methods.

Second, I establish self-similar solutions and their scaling properties. For Gaussian diffusion from instantaneous point sources, boundaries expand as $d^*(t) = \xi^* \sqrt{t}$ where the scaling coefficient $\xi^* = 2\sqrt{\nu \ln(1/(1 - \varepsilon))}$ depends on both the diffusion coefficient ν and the threshold parameter ε . The boundary velocity $v(t) = \xi^*/(2\sqrt{t})$ decelerates over time, reflecting the fundamental physics of diffusion. This is in sharp contrast to linear expansion that would characterize advection-dominated transport.

Third, I develop the analytical framework for parameter sensitivity and cumulative exposure. The boundary elasticity with respect to diffusion coefficient is constant at $\partial \ln d^* / \partial \ln \nu = 0.5$, enabling straightforward policy counterfactuals. A 20 percent increase in effective diffusion coefficient (e.g., via transportation improvements) yields a 9.5 percent boundary expansion. Cumulative exposure $\Phi(\mathbf{x}) = \int_0^T \tau(\mathbf{x}, t) dt$ integrates treatment intensity over time, providing a welfare-relevant measure for cost-benefit analysis.

7.3 Methodological Contributions

The methodological contributions center on diagnostic procedures and model selection.

Diagnostic capability distinguishes this framework from traditional spatial econometric methods. The sign reversal test is simple yet powerful: estimate κ and test whether $\kappa > 0$. Positive values validate diffusion assumptions; zero or negative values signal that the framework does not apply due to confounding or alternative mechanisms. This diagnostic worked as intended in the empirical application: ACCESS2 showed positive decay (framework applies), while BPHIGH showed zero decay (framework correctly rejects). This prevents mechanical application of the framework to settings where underlying assumptions fail.

Model selection procedures address a fundamental question: which functional form best describes spatial decay? I compare exponential, power-law, and logarithmic specifications using AIC and BIC. The overwhelming evidence for logarithmic decay (difference in AIC exceeding 15,000) suggests that diminishing marginal effects characterize spatial treatment propagation for healthcare access. This finding likely generalizes to other settings where initial proximity matters most: banking services, retail access, public goods provision. The implication is that researchers should not automatically assume exponential decay but should test alternative specifications.

Heterogeneity analysis within the continuous functional framework enables decomposition of treatment effects by demographic characteristics while maintaining the continuous spatial structure. Traditional methods estimate separate treatment effects for discrete subgroups within arbitrary distance bands. The continuous functional approach estimates separate decay parameters κ_g for each group g , providing interpretable ratios $\kappa_{high}/\kappa_{low}$ that measure relative decay rates. This approach is more parsimonious (two parameters per group rather than many distance band coefficients) and more interpretable (a single ratio captures the relative importance of distance across groups).

7.4 Comparison to Related Literatures

This framework relates to several literatures while offering distinct advantages.

Compared to spatial econometrics (Anselin 1988, Conley 1999, Mueller and Watson 2022, 2024), the continuous functional approach derives spatial correlation structure from physical principles rather than imposing it statistically. Traditional spatial econometrics estimates spatial lag models, spatial error models, or applies spatial HAC standard errors. These methods treat spatial correlation as a nuisance parameter to be controlled. In contrast, the continuous functional framework models spatial correlation as the object of interest, emerging from underlying diffusion processes. This provides interpretable parameters (κ, ν, d^*) with direct policy relevance.

Compared to treatment effect heterogeneity literature (Imbens and Rubin 2015, Athey and Imbens 2017, Chernozhukov et al. 2018), the framework provides continuous rather than discrete heterogeneity. Traditional methods estimate conditional average treatment effects (CATE) as functions of covariates using machine learning. These are fundamentally discrete—separate treatment effects for different covariate values. The continuous functional approach provides spatially continuous treatment intensity $\tau(\mathbf{x}, t)$ and gradients $\nabla \tau$ measuring the intensive margin. This enables analysis of where effects change most rapidly, crucial for targeting interventions.

Compared to difference-in-differences with spatial spillovers (Butts and Gardner 2023), the framework provides explicit functional forms rather than nonparametric spillover estimates. Recent DiD methods allow for spillovers by including neighbors' treatment status in the regression. However, these methods typically do not specify functional forms for spillover decay, instead estimating separate coefficients for distance bands. The continuous functional approach provides parametric decay functions enabling extrapolation and

counterfactual analysis.

Compared to my own prior work, this paper provides comprehensive empirical validation across multiple health outcomes with detailed model comparison. Kikuchi (2024a) established the unified theoretical framework; this paper demonstrates empirical applicability. Kikuchi (2024d,e) developed nonparametric methods; this paper shows parametric specifications often outperform nonparametric when functional form is correctly specified (logarithmic vs exponential). Kikuchi (2024c) focused on dynamic panel data; this paper emphasizes cross-sectional analysis with detailed heterogeneity decomposition.

7.5 Policy Implications

The framework provides four types of policy guidance unavailable in traditional approaches.

First, facility placement guidance. Rather than arbitrary distance cutoffs (e.g., "ensure all populations are within 50 miles of a hospital"), the framework identifies data-driven boundaries. For ACCESS2, the 37 km boundary suggests new hospitals should target areas beyond this threshold to maximize impact on uninsured rates. Areas within 37 km are already in the treatment zone; areas beyond 37 km face meaningful access barriers. This precision improves resource allocation compared to ad hoc cutoffs.

Second, transportation program targeting. The continuous decay function reveals where effects are largest. For ACCESS2 with logarithmic decay, the steepest gradient occurs at moderate distances (20-60 km) rather than extremely remote areas. Transportation assistance programs should prioritize this range where diminishing returns are not yet severe. Extremely remote populations (beyond 150 km) show minimal sensitivity to transportation improvements because distance is not the binding constraint—other factors (income, insurance policy, local supply) dominate.

Third, heterogeneity-based targeting. The finding that education reduces distance sensitivity 5-13 times suggests that health literacy programs can partially substitute for physical proximity. For low-education populations, traditional interventions (transportation, mobile clinics) are essential. For high-education populations, telemedicine with minimal additional support suffices. The framework quantifies these trade-offs enabling cost-benefit optimization.

Fourth, policy counterfactual analysis. The parameter sensitivity $\partial d^* / \partial \nu = d^* / (2\nu)$ enables computing the effect of policy interventions that increase effective diffusion. A transportation improvement increasing ν by 20 percent expands the boundary by 3.5 km. If per-capita benefit is B dollars and population density is ρ people per square km, total benefit equals $B \cdot \rho \cdot 4\pi(d^*)^2 \cdot \Delta d^*$ where $\Delta d^* = 3.5$ km. Comparing this to program cost yields a cost-benefit ratio guiding budget allocation.

7.6 Limitations and Future Research

Five limitations suggest directions for future research.

First, low overall explanatory power ($R^2 = 0.01-0.02$) indicates distance is a modest determinant of healthcare access. Other factors—insurance policy, income, employment, local supply—explain 98-99 percent of variation. However, this does not diminish policy relevance: distance is manipulable via hospital placement and transportation programs, while income and insurance policy operate through different channels. The framework identifies the causal effect of distance conditional on other factors. Future work should incorporate these other determinants explicitly, perhaps through spatial general equilibrium models where hospital placement affects local economic activity (Kikuchi 2024b).

Second, synthetic demographic data limits heterogeneity analysis precision. I gen-

erated synthetic Census data to demonstrate the framework’s heterogeneity analysis capabilities. Real Census data at the ZCTA level would enable more precise estimates of age, education, and income effects. Future work should incorporate American Community Survey microdata or restricted-use Census data. This would allow finer demographic breakdowns: not just ”elderly” vs ”young” but detailed age profiles; not just ”high education” vs ”low education” but precise educational attainment distributions.

Third, cross-sectional design prevents causal identification beyond conditional correlations. The framework identifies spatial decay patterns but cannot definitively establish that hospital proximity causes improved access (as opposed to hospitals locating near populations with good access for other reasons). Panel data exploiting hospital openings and closures would enable difference-in-differences estimation within the continuous functional framework (Kikuchi 2024c). Combining panel methods with the spatial decay framework would strengthen causal inference.

Fourth, Euclidean distance abstracts from transportation networks. Haversine distance assumes agents can travel in straight lines, ignoring roads, mountains, and other geographic barriers. Road network distance or travel time would better capture effective accessibility. Future work should incorporate network distance, perhaps through graph-based diffusion models where treatment propagates along edges (roads) rather than through continuous space. This would be particularly important for rural areas where road networks are sparse.

Fifth, hospital quality is unobserved. Distance to the nearest hospital ignores quality variation: a nearby low-quality facility may be less valuable than a distant high-quality center. Future work should incorporate quality measures: hospital ratings, physician density, technology availability, specialties offered. This requires extending the framework to multiple

sources with heterogeneous intensities: $\tau(\mathbf{x}) = \sum_j Q_j \exp(-\kappa|\mathbf{x} - \mathbf{x}_j|)$ where Q_j reflects quality of hospital j . Quality-distance trade-offs could then be quantified.

7.7 Broader Implications

Beyond healthcare, the continuous functional framework applies to many settings where treatments propagate spatially from point sources.

Environmental economics: Pollution emissions from factories disperse according to atmospheric diffusion. The framework identifies boundaries of environmental impact zones, enabling optimal siting decisions and damage assessments. Kikuchi (2024d) demonstrates this with 42 million air quality observations, finding boundaries of 50-150 km depending on pollutant and weather conditions.

Banking and finance: Bank branch networks provide spatially localized services. The framework measures the effective reach of branches, guiding expansion and consolidation decisions. Kikuchi (2024e) applies nonparametric boundary identification to branch closures, finding that urban confounding creates negative decay parameters—branches locate in high-quality areas rather than causing high quality.

Technology diffusion: Innovations spread through space via peer effects and local information networks. The framework characterizes diffusion patterns, enabling prediction of adoption trajectories. Social learning may exhibit power-law rather than exponential decay if long-range connections matter.

Infrastructure and public goods: Schools, libraries, parks, transit stations provide localized benefits. The framework identifies optimal facility spacing by balancing coverage (minimize distances) against cost (fixed costs per facility). This is a classic location-allocation problem, now informed by empirically estimated decay functions.

Retail and services: Stores, restaurants, and consumer services face spatial competition and decay of demand with distance. The framework informs site selection and pricing strategies by quantifying effective market reach. This connects to spatial competition models in industrial organization.

The common thread is spatial propagation from discrete sources. Whenever treatment effects can be conceptualized as diffusing through space, the continuous functional framework applies. The key requirement is identifiable point sources; for diffuse or network-based treatments, alternative approaches are needed.

7.8 Final Remarks

This paper demonstrates that continuous functional methods from mathematical physics can advance empirical economics. By characterizing treatment effects as fields $\tau(\mathbf{x}, t)$ satisfying PDEs, we gain access to powerful analytical tools: calculus for gradients and integrals, self-similar solutions for scaling laws, parameter sensitivity for counterfactuals. These are unavailable in traditional discrete frameworks.

The cost is additional structure: diffusion mechanism, parametric functional forms, point source assumptions. The benefit is predictive capability, parameter interpretation, and diagnostic tests. The empirical validation shows this trade-off is favorable for healthcare access. Model selection reveals that careful specification search (logarithmic vs exponential vs power-law) is critical—mechanical application of exponential decay would miss important features (diminishing marginal effects).

Looking forward, continuous functional methods should become part of the spatial econometrician’s toolkit alongside traditional methods. They are not replacements but complements: use continuous functionals when physical mechanisms are clear and point sources

are identifiable; use traditional methods for robustness and when mechanisms are opaque. The ideal empirical strategy combines both approaches, with agreement strengthening conclusions and disagreement revealing which assumptions drive results.

The framework’s success in identifying boundaries ($d^* = 37$ km for healthcare access), validating functional forms (logarithmic over exponential by decisive margin), and diagnosing scope conditions (positive decay for ACCESS2, zero for BPHIGH) suggests broad applicability. Future work extending to panel data, network distance, quality variation, and general equilibrium feedbacks promises to deepen our understanding of how treatments propagate through space and time.

Ultimately, spatial treatment effects are inherently continuous—they do not jump discontinuously at arbitrary cutoffs. Economic theory, empirical evidence, and policy relevance all point toward continuous functional frameworks as the natural approach to spatial causal inference. This paper takes an initial step in that direction, demonstrating feasibility and value. Much work remains to fully develop the continuous functional paradigm, but the foundations are now in place.

References

Allen, T., & Arkolakis, C. (2014). Trade and the topography of the spatial economy. *Quarterly Journal of Economics*, 129(3), 1085–1140.

Anselin, L. (1988). *Spatial Econometrics: Methods and Models*. Springer-Verlag.

Athey, S., & Imbens, G. W. (2017). The econometrics of randomized experiments. *Handbook of Economic Field Experiments*, 1, 73–140.

Buchmueller, T. C., Jacobson, M., & Wold, C. (2006). How far to the hospital? The effect of hospital closures on access to care. *Journal of Health Economics*, 25(4), 740–761.

Butts, K., & Gardner, J. (2023). Difference-in-differences with spatial spillovers. Working paper.

Chernozhukov, V., Chetverikov, D., Demirer, M., Duflo, E., Hansen, C., Newey, W., & Robins, J. (2018). Double/debiased machine learning for treatment and structural parameters. *Econometrics Journal*, 21(1), C1–C68.

Cliff, A. D., & Ord, J. K. (1981). *Spatial Processes: Models and Applications*. Pion.

Conley, T. G. (1999). GMM estimation with cross sectional dependence. *Journal of Econometrics*, 92(1), 1–45.

Crank, J. (1979). *The Mathematics of Diffusion* (2nd ed.). Oxford University Press.

Currie, J., & Neidell, M. (2005). Air pollution and infant health: What can we learn from California’s recent experience? *Quarterly Journal of Economics*, 120(3), 1003–1030.

Currie, J., & Reagan, P. (2003). Distance to hospital and children's access to care. *Journal of Health Economics*, 22(6), 1005–1027.

Delgado, M. S., & Robinson, P. M. (2014). Testing for a unit root in spatial models. Working paper.

Delgado, M., Florens, J. P., & Protopopescu, C. (2021). Bounds for treatment effects under sample selection and spatial correlation. Working paper.

Evans, L. C. (2010). *Partial Differential Equations* (2nd ed.). American Mathematical Society.

Heblich, S., Trew, A., & Zylberberg, Y. (2021). East-side story: Historical pollution and persistent neighborhood sorting. *Journal of Political Economy*, 129(5), 1508–1552.

Hsiang, S., Kopp, R., Jina, A., Rising, J., Delgado, M., Mohan, S., ... & Houser, T. (2019). Estimating economic damage from climate change in the United States. *Science*, 356(6345), 1362–1369.

Imbens, G. W., & Rubin, D. B. (2015). *Causal Inference for Statistics, Social, and Biomedical Sciences*. Cambridge University Press.

Kelly, B. T., Pruitt, S., & Su, Y. (2019). Characteristics are covariances: A unified model of risk and return. *Journal of Financial Economics*, 134(3), 501–524.

Kikuchi, T. (2024a). A unified framework for spatial and temporal treatment effect boundaries: Theory and identification. *arXiv preprint arXiv:2510.00754*.

Kikuchi, T. (2024b). Stochastic boundaries in spatial general equilibrium: A diffusion-based approach to causal inference with spillover effects. *arXiv preprint arXiv:2508.06594*.

Kikuchi, T. (2024c). Spatial and temporal boundaries in difference-in-differences: A framework from Navier-Stokes equation. *arXiv preprint arXiv:2510.11013*.

Kikuchi, T. (2024d). Nonparametric identification and estimation of spatial treatment effect boundaries: Evidence from 42 million pollution observations. *arXiv preprint arXiv:2510.12289*.

Kikuchi, T. (2024e). Nonparametric identification of spatial treatment effect boundaries: Evidence from bank branch consolidation. *arXiv preprint arXiv:2510.13148*.

Kikuchi, T. (2024f). Dynamic spatial treatment effect boundaries: A continuous functional framework from Navier-Stokes equations. *arXiv preprint arXiv:2510.14409*.

Monte, F., Redding, S. J., & Rossi-Hansberg, E. (2018). Commuting, migration, and local employment elasticities. *American Economic Review*, 108(12), 3855–3890.

Müller, U. K., & Watson, M. W. (2022). Spatial correlation robust inference. *Econometrica*, 90(6), 2901–2935.

Müller, U. K., & Watson, M. W. (2024). Spatial unit roots and spurious regression. *Econometrica*, 92(5), 1661–1695.

Redding, S. J., & Rossi-Hansberg, E. (2017). Quantitative spatial economics. *Annual Review of Economics*, 9, 21–58.